AD NUMBER

ADB011353

LIMITATION CHANGES

TO:

Approved for public release; distribution is unlimited.

FROM:

Distribution authorized to U.S. Gov't. agencies only; Test and Evaluation; 11 SEP 1975. Other requests shall be referred to Air Force Cambrige Research Laboratories, Hanscon AFB, MA 01731.

AUTHORITY

USAFGL ltr, 1 Aug 1983

AFCRL-TR-75-0481
AIR FORCE SURVEYS IN GEOPHYSICS, NO. 323

Final Report of PVM-6 and PVM-7 Weather Documentation

AFCRL/Minuteman Report No. 6

JAMES I. METCALF, Capt, USAF
MICHAEL J. KRAUS
ARNOLD A. BARNES, Jr.

11 September 1975

METEOROLOGY LABORATORY PROJECT 1338
AIR FORCE CAMBRIDGE RESEARCH LABORATORIES
HANSCOM AFB, MASSACHUSETTS 01731

AIR FORCE SYSTEMS COMMAND, USAF

Unclassified

SECURITY CLASSIFICATION OF THIS PAGE (When Data Entered)

REPORT DOCUMENTATION PAGE

READ INSTRUCTIONS BEFORE COMPLETING FORM

1. REPORT NUMBER: AFCRL-TR-75-0481	2. GOVT ACCESSION NO.: AFCRL-AFSG-323
3. RECIPIENT'S CATALOG NUMBER	
4. TITLE (and Subtitle): FINAL REPORT OF PVM-6 AND PVM-7 WEATHER DOCUMENTATION; AFCRL/Minuteman Report [redacted] Number 6.	5. TYPE OF REPORT & PERIOD COVERED: Scientific. Interim.
	6. PERFORMING ORG. REPORT NUMBER: AFSG No. 323 ✓
7. AUTHOR(s): James I. Metcalf, Capt, USAF; Michael J. Kraus; Arnold A. Barnes, Jr	8. CONTRACT OR GRANT NUMBER(s)
9. PERFORMING ORGANIZATION NAME AND ADDRESS: Air Force Cambridge Research Laboratories(LYW) Hanscom AFB Massachusetts 01731	10. PROGRAM ELEMENT, PROJECT, TASK AREA & WORK UNIT NUMBERS: AF - 133B0001 11213F
11. CONTROLLING OFFICE NAME AND ADDRESS: Air Force Cambridge Research Laboratories(LYW) Hanscom AFB Massachusetts 01731	12. REPORT DATE: 11 Sep [redacted]75; 13. NUMBER OF PAGES: 58
14. MONITORING AGENCY NAME & ADDRESS (if different from Controlling Office)	15. SECURITY CLASS. (of this report): Unclassified; 15a. DECLASSIFICATION/DOWNGRADING SCHEDULE

16. DISTRIBUTION STATEMENT (of this Report)

Distribution limited to U.S. Government agencies only; (Test and Evaluation; [redacted]; (11 September 1975). Other requests for this document must be referred to AFCRL/LYW, Hanscom AFB, Massachusetts 01731.

17. DISTRIBUTION STATEMENT (of the abstract entered in Block 20, if different from Report)

Air Force surveys in geophysics,

18. SUPPLEMENTARY NOTES

19. KEY WORDS (Continue on reverse side if necessary and identify by block number)

Minuteman
Aircraft weather measurement
Radar weather measurement
Tropical cirrus clouds
Water content profiles

20. ABSTRACT (Continue on reverse side if necessary and identify by block number)

Reentry weather measurements conducted under the Minuteman Natural Hazards Program are described. The missions described here are PVM-6 and PVM-7, which were postured to reenter through "heavy weather." Documentation was accomplished primarily by instrumented C-130E and Cessna Citation aircraft, by high-power radar, and by satellite. The weather objective was met in a qualitative sense, in that the vehicles reentered through a thick cloud mass that was remarkably uniform horizontally in the reentry corridor.

DD FORM 1 JAN 73 1473 EDITION OF 1 NOV 65 IS OBSOLETE

Unclassified

SECURITY CLASSIFICATION OF THIS PAGE (When Data Entered)

next page

Unclassified

SECURITY CLASSIFICATION OF THIS PAGE(When Data Entered)

20. Abstract (Continued)

The Weather Severity Indices (WSI) for the PVM-6 trajectories were 4.3, 5.9, and 3.6 for RV's 1, 2, and 3. The weather system was weakening by the time of the PVM-7 reentry, so that the WSI was 2.0 and 1.6 for RV's 1 and 2.

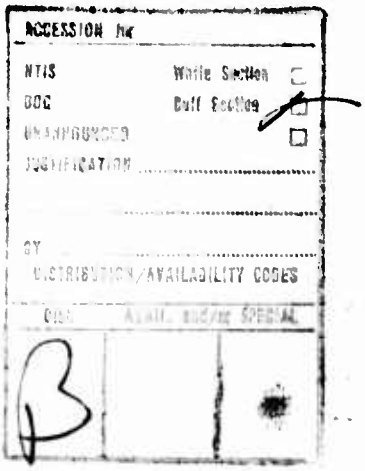

Unclassified

SECURITY CLASSIFICATION OF THIS PAGE(When Data Entered)

Preface

Field work at Kwajalein Missile Range under the Minuteman Natural Hazards Program was conducted from 17 July through 24 August and 2 September through 14 October 1974. One of the primary objectives of this field project was the documentation of reentry weather for two missile tests intended for reentry through thick clouds. These tests, designated PVM-6 and PVM-7, were launched on 12 October 1974 into a weather system that produced widespread clouds in the Kwajalein area.

The field support included representatives of SAMSO/MN; SAMTEC/WE; 6th Weather Wing; AFSWC; AFCRL Meteorology Laboratory; FAA; TRW Systems Group; Meteorology Research, Inc.; Science Applications, Inc.; Particle Measuring Systems, Inc.; and Alpine Air Charter. TRW was responsible for the overall planning and operation of the weather program.[1] The roles of the other organizations are described in our report. MRI was responsible for the operation of the instrumentation on the Citation aircraft (except the holographic camera); readers interested in more details of the equipment or data than are presented

1. Wilmot, R.A., Cisneros, C.E., and Guiberson, F.L. (1974) High cloud measurements applicable to ballistic missile systems testing, 6th Conf. Aerosp. and Aeronaut. Meteor., Amer. Meteor. Soc., 194-199.

here are referred to their final report.[2] The holographic camera is described in the SAI final report[3] and in a special MRI report.[4]

Reports prepared to date in the AFCRL/Minuteman Series are as follows:

1. Aircraft and Radar Data Analysis for PVM-5 (AFCRL-TR-74-0627, 23 Dec 1974) AD-B004 290L.
2. Final Report of PVM-4 and PVM-3 Weather Documentation (AFCRL-TR-75-0097, 14 Feb 1975) AD-B004 427L.
3. Final Report of STM-8W Weather Documentation (AFCRL-TR-75-0207, 11 April 1975) AD-B006 666L.
4. Final Report of PVM-5 Weather Documentation (AFCRL-TR-75-0302, 28 May 1975) AD-B006 667L.
5. Final Report of OT-45, PVM-8 and RVTO Weather Documentation (AFCRL-TR-75-0388, 23 July 1975) AD-B011 352L.

---

2. Jahnsen, L.J., and Heymsfield, A.J. (1975) High Altitude Ice Cloud Characterization: PVM-6, -7, and -8 Missions, MRI 75 FR-1350, Meteorology Research, Inc., Altadena, California.
3. Trolinger, J.D., Farmer, W.M., and Clayton, F.P. (1974) Development and Application of an Airborne Holography System and Particle Sizing Interferometer, SAI-74-511-TT, Science Applications, Inc., La Jolla, California.
4. Jahnsen, L.J. (1975) Utilization of SAMSO Airborne Holocamera for Cloud Physics Measurements, MRI 75 FR-1331, Meteorology Research, Inc., Altadena, California.

Contents

Illustrations

Tables

Final Report of PVM-6 and PVM-7 Weather Documentation

AFCRL/Minuteman Report No. 6

I. INTRODUCTION

The PVM-6 and PVM-7 missions were launched on 12 October 1974, with reentry near Kwajalein Atoll at 0523 and 0804Z, respectively. The "heavy weather" criterion for both missions was satisfied. This report describes the weather data acquisition plan and presents our final determination of the water content profiles encounted by the reentry vehicles. Data from the various meteorological sensors are presented to provide further details on the weather in the vicinity of the targets.

Descriptions of each of the sensors are included with the presentations of data in the following sections. The locations of the supporting facilities are shown in Figure 1. The NWS rawinsonde and weather radar facilities and the DMSP satellite van operated by the 6th Weather Wing from McClellan AFB were located on Kwajalein Island. The Lincoln Laboratory tracking radars, located at KREMS on Roi-Namur Island, were used to obtain weather data on the reentry trajectories. NWS rawinsonde facilities at Roi-Namur were used for soundings in conjunction with the missions, in addition to the soundings from Kwajalein. A C-130E aircraft, operated by AFSWC from Kirtland AFB and instrumented for cloud physics measurements by AFCRL, and a Cessna Citation aircraft, operated

(Received for publication 10 September 1975)

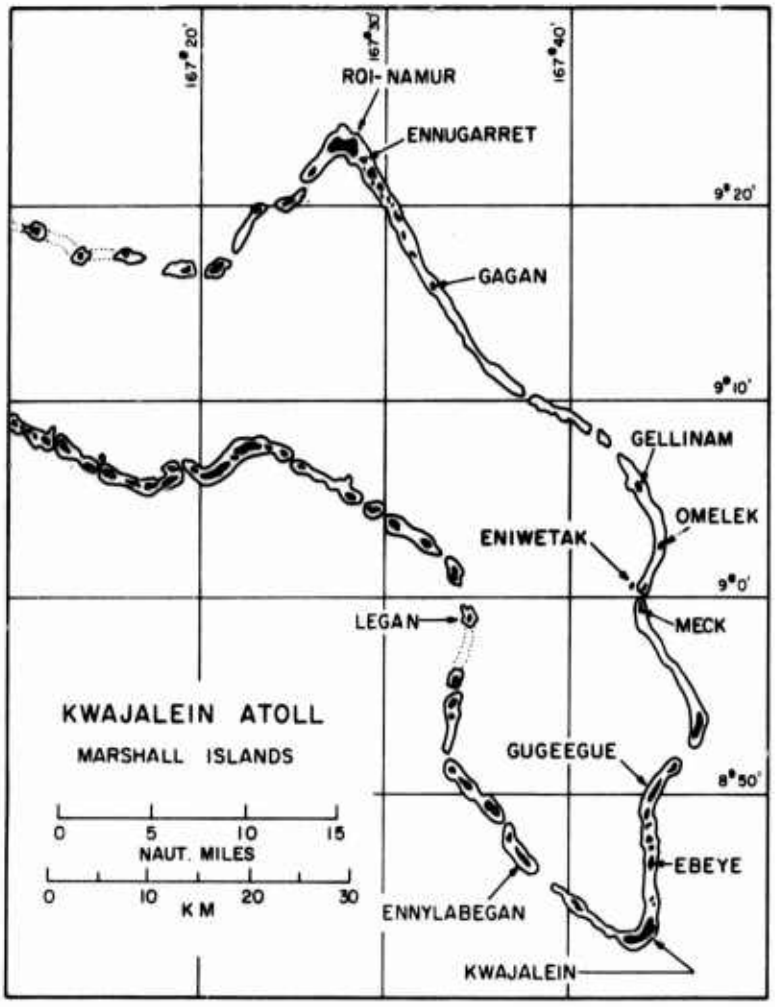

Figure 1. Kwajalein Atoll, Showing the Islands Occupied by the Facilities of Kwajalein Missile Range. Range Operations Control Center, aircraft support facilities, NWS radars, and MPS-36 radars are at Kwajalein Island. Lincoln Laboratory radars are at Roi-Namur Island. Telemetry and optical tracking stations are located on other islands.

by Alpine Air Charter and instrumented by MRI, were based at Kawajalein during the July-October field program and performed weather sampling in support of the PVM-6 and PVM-7 test objectives. The joint aircraft operations were under the control of an aircraft vector controller from the FAA.

Execution of the weather data acquisition plan and on-site evaluation of the data were the responsibilities of the mission weather team. The weather team

included representatives of SAMSO, SAMTEC, TRW, and MRI at the ROCC and an AFCRL radar meteorologist at KREMS. An AFCRL meteorological flight director and two AFCRL instrumentation technicians flew on the C-130E.

The reentry weather was defined in terms of the Weather Severity Index

$$WSI = \int_{h_1}^{h_2} M\, h\, dh \tag{1}$$

where h_1 is the height (km) of the lowest cloud base and h_2 is the height of the highest cloud top on the trajectory. For numerical integration across a thick cloud layer this may be approximated by

$$WSI \cong \sum_i M_i \bar{h}_i \Delta h_i \tag{2}$$

$$\cong \sum_i M_i \frac{(h_i + h_{i-1})}{2} (h_i - h_{i-1})$$

$$= \sum_i M_i \frac{(h_i^2 - h_{i-1}^2)}{2} \quad . \tag{3}$$

The nominal criterion for these missions was WSI> 8.

All the reentry vehicles passed through a thick cloud layer. Cloud top was near 12.5 km, and cloud base was below 3 km in all cases. Maximum water content of 0.30 gm m^{-3} was observed at 5.0 km on the PVM-6 RV2 trajectory. Maximum water content on the PVM-7 trajectories was about 0.11 gm m^{-3}, observed near 4.6 km. The WSI's were 4.3, 5.9, and 3.6 for PVM-6 RV's 1, 2, and 3, and 2.0 and 1.6 for PVM-7 RV's 1 and 2. The Citation made two flights prior to PVM-6 and one flight after PVM-6 which extended to just after PVM-7 reentry. These flights were primarily for cloud sampling in the reentry corridor, which was accomplished in a series of ascents and descents between 4 and 12 km altitude. The C-130E made one 4-hr flight prior to PVM-6 to sample clouds in the reentry corridor and in a region southeast of the corridor. A 4.5-hr flight by the C-130E following the PVM-6 reentry included a descent in the reentry corridor after the PVM-7 reentry and a series of passes for correlation with ALCOR.

2. WEATHER DESCRIPTION

Occurrences of widespread cloudiness over the tropical Pacific are generally associated with the inter-tropical convergence zone (ITCZ). At the longitude of Kwajalein the axis of the ITCZ varies between 3°N and 16°N latitude, with particularly rapid southward movement during October[5]. Climatological studies[6] show that the rainfall and cloud cover at Kwajalein are associated with this migration of the ITCZ. Figure 2 shows that the maximum mean monthly rainfall occurs in October, in conjunction with the southward movement of the ITCZ.

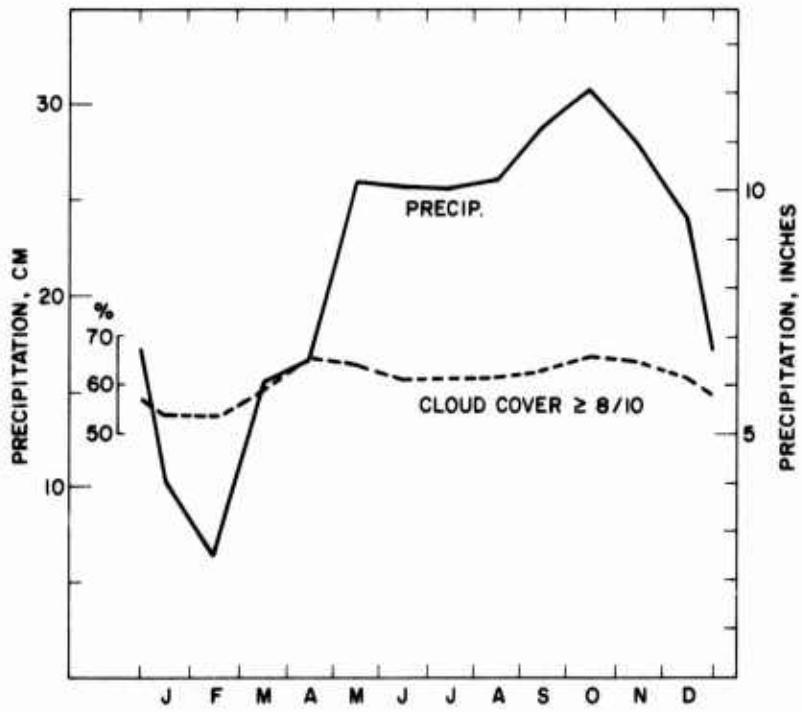

Figure 2. Mean Monthly Precipitation (1945-1972) and Cloud Cover (1946-1972) at Kwajalein. "Wet season" is from mid-May to mid-December, with peak precipitation in October.

5. Gruber, A. (1972) Fluctuations in the position of the ITCZ in the Atlantic and Pacific Oceans, J. Atmos. Sci. 29:193-197.

6. USAF Environmental Technical Applications Center (1973) Monthly Cloud Climatology for Kwajalein, Marshall Islands. Project 7076, Report 7076A.

A major weather system developing along the ITCZ produced widespread cloudiness in the Kwajalein area at the time of the PVM-6 and PVM-7 reentries. At 1200Z on 11 October the 250-mb analysis showed that Kwajalein was on the southern side of a broad low pressure trough, with a minor trough about 1200 km to the west. A low pressure trough at the surface had moved over Kwajalein about 12 hr earlier, and was centered about 300 km to the west at 1200Z. Convective activity associated with the low pressure system was beginning to produce high-level cirrus at this time. During the next 12 hr the weather system developed rapidly. The upper-level trough deepened, and a closed low pressure center was located about 700 km west-southwest of Kwajalein at 0000Z on 12 October. The cirrus was extensive and quite thick in an east-west band 600 km wide over Kwajalein. These clouds persisted through the time of the reentries, as shown in Figure 3, although there were indications that the clouds were beginning to dissipate by the time of the PVM-7 reentry.

The National Weather Service provided data from the WSR-57 weather radar and from rawinsondes. The TPQ-11 radar was not operational on this day. At the time of the PVM-6 reentry the WSR-57 detected widespread precipitation echoes in and near the reentry corridor, as shown in Figure 4. Movement of the cells was difficult to determine, due to their evolution, but was very slight, less than 5 m sec^{-1} from the south. RHI scans near the time of the reentry at azimuths between 14° and 354° (moving counterclockwise) showed that the echo tops were near 5.5 km. The decrease in convective activity is illustrated dramatically in Figure 5, which shows only individual cells or small groups of cells at the time of PVM-7 reentry. The weak echoes at 145 km range and 340° azimuth were the remnants of the large echo that was in this area 3 hr earlier (Figure 4). The cell at 70 km range and 5° azimuth was first detected about 0730Z at 55 km range. It developed rapidly, moving slowly northward, but did not extend higher than 5.8 km at the time of reentry. The RHI scans revealed no echoes higher than 3 km, with the exception of the one cell just described. This precipitation cell was imbedded in a rather uniform ice crystal cloud layer that the WSR-57 could not detect, but which was observed by the aircraft and by ALCOR.

Rawinsondes were released from Kwajalein at 0525 and 0802Z and from Roi-Namur at 0625 and 0802Z. (The 0625Z sounding was the second release from Roi-Namur, because the first PVM-6 sounding from Roi-Namur had failed to penetrate the cloud layer due to icing of the balloon.) The wind and thermal structures shown by all these soundings were similar, although there were some changes during the 3-hr period and some differences between Kwajalein and Roi-Namur. The most striking feature was the relatively high humidity at all levels, associated with the thick clouds. The PVM-6 soundings (Figure 6) showed relative humidity greater than 75 percent from the surface to nearly 10 km, and 90 percent or more

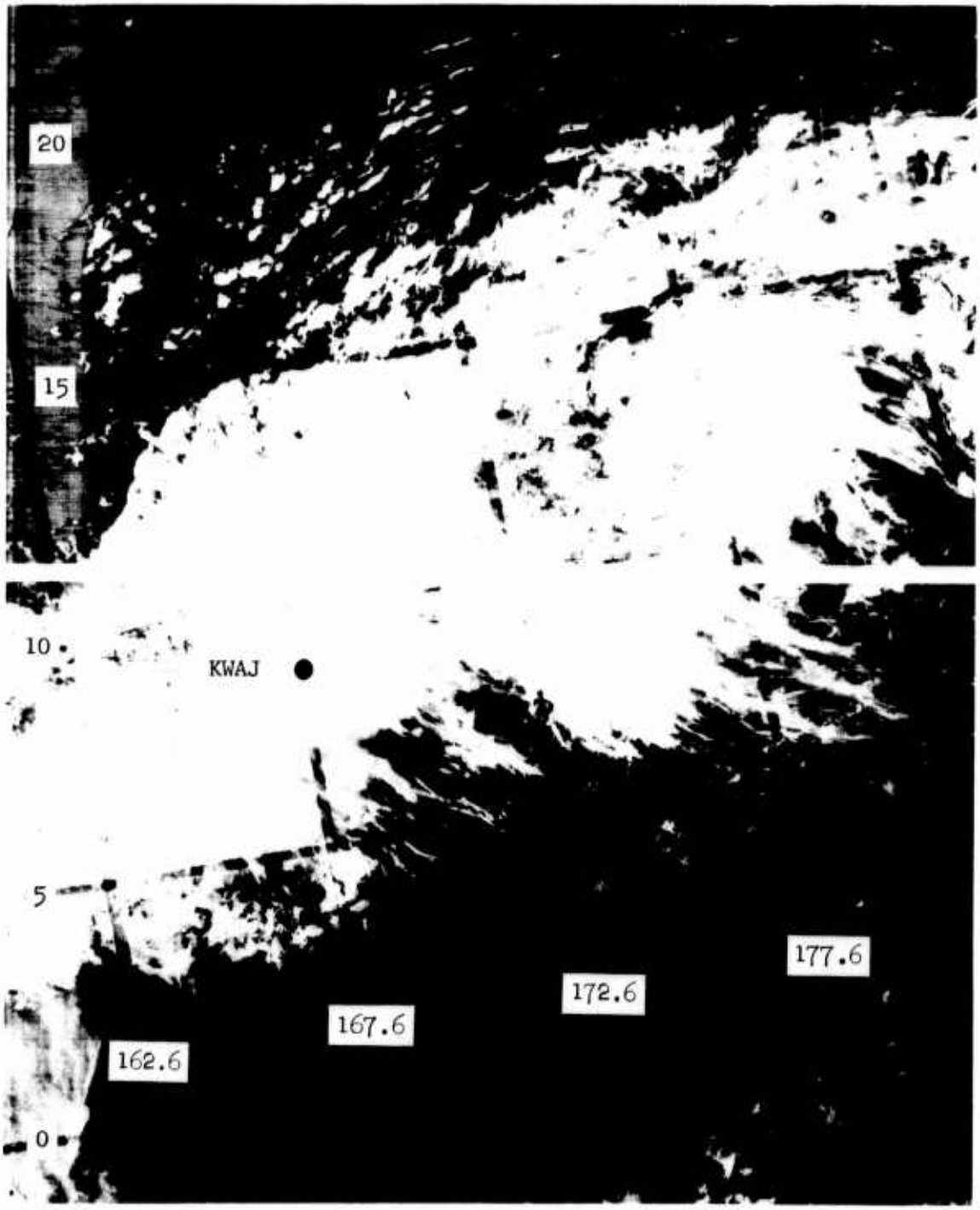

Figure 3. DMSP Satellite Visual Data for 12 October 1974, 0731Z. Cloud band is associated with a major weather system centered about 700 km west-southwest of Kwajalein. The highest clouds were moving toward the east at speeds of 5 to 10 m sec^{-1}. These clouds first developed some 15 to 20 hr earlier, and were beginning to dissipate at the time of this picture.

Figure 4. WSR-57 Radar PPI Display at 0506Z, 12 October 1974. Elevation angle is 0^{o} and range markers are at 25 nmi (46.3 km) intervals out to 125 nmi (231.5 km). Echoes from the atoll islands are seen to the north and northwest to about 35 km range. Major precipitation areas are detected 40 to 110 km to the east and 65 to 200 km to the north and northwest.

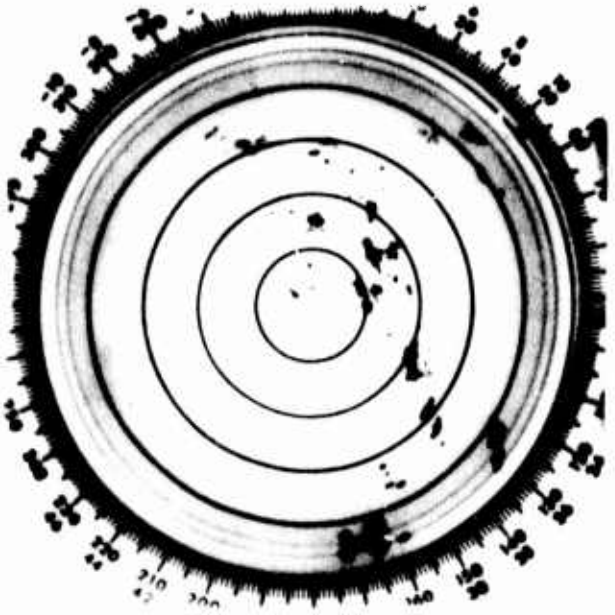

Figure 5. WSR-57 Radar PPI Display at 0815Z, 12 October 1974. Format is identical to that of Figure 4. Isolated precipitation cells or groups of cells are detected at 40 to 100 km range to the east and northeast, and one major cell is near the reentry corridor at 70 km north of Kwajalein.

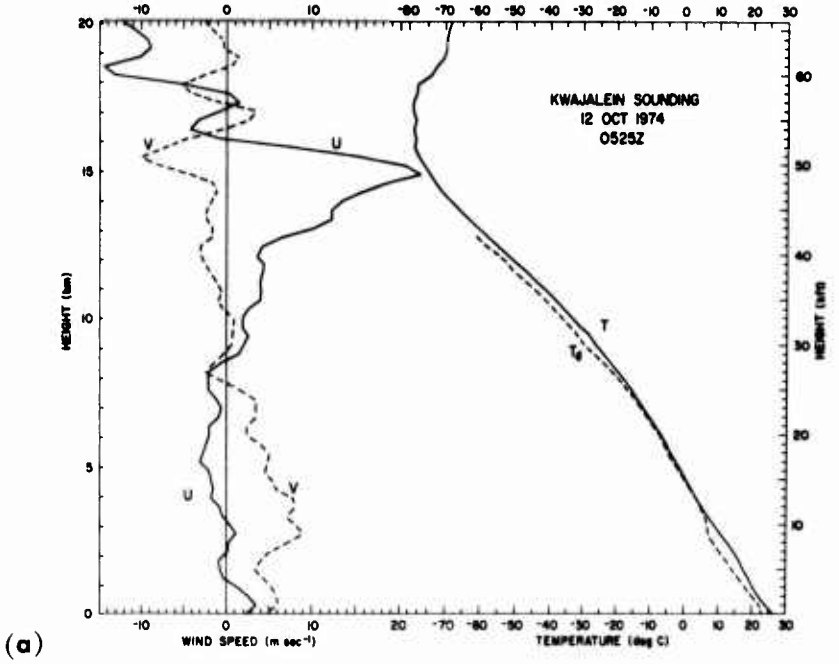

(a)

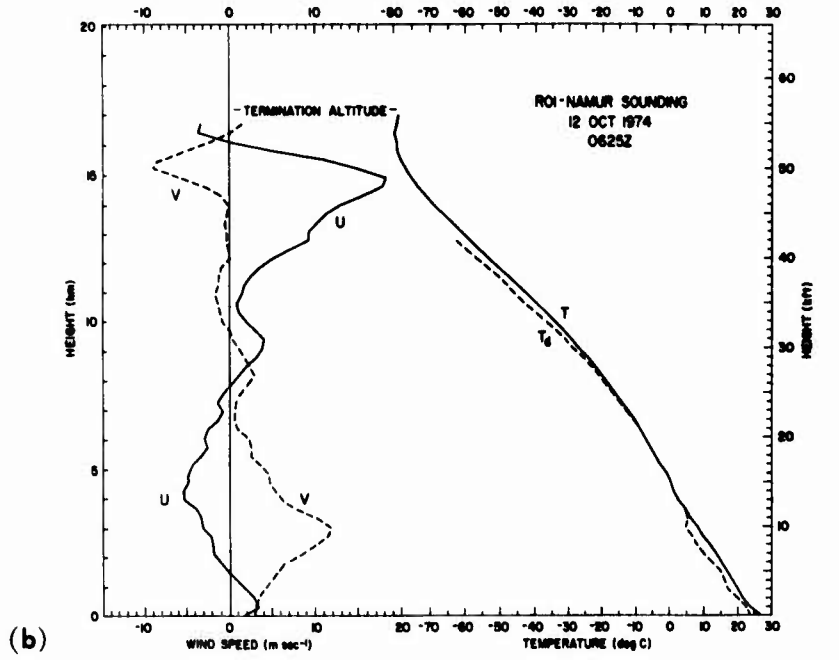

(b)

Figure 6. Soundings From (a) Kwajalein at 0525Z and (b) Roi-Namur at 0625Z, 12 October 1974. Wind components are plotted toward the east (U) and toward the north (V). Low-level winds are from the south, backing to southeasterly near 5 to 6 km altitude. In the upper part of the cloud layer, at 10 to 13 km, the wind is westerly, veering to northwesterly just below the tropopause at 17 km. Humidity is high at all levels.

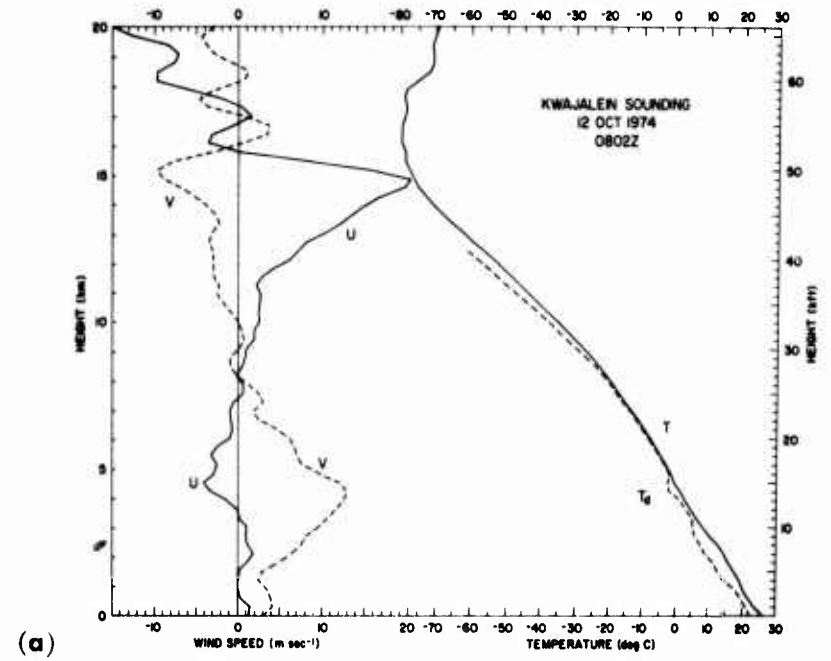

(a)

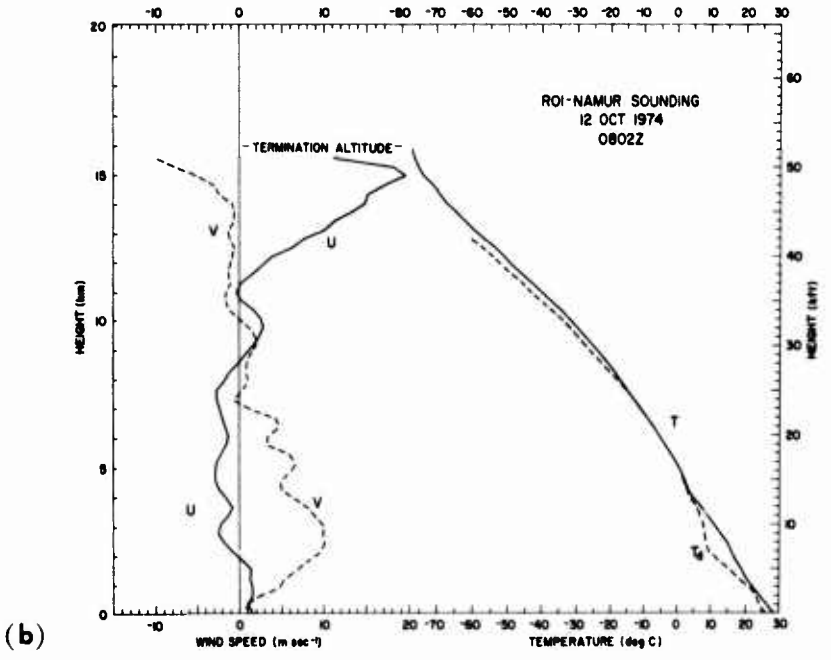

(b)

Figure 7. Soundings From (a) Kwajalein and (b) Roi-Namur at 0802Z, 12 October 1974. Format is identical to that of Figure 6. Features of the wind and temperature structure are similar to those shown in Figure 6.

between 3.4 and about 8 km; the Roi-Namur sounding measured saturation humidity (100 percent) between 3.7 and 6.4 km. The freezing level at this time was at 4.7 km, and the tropopause was near 17 km. Surface winds were from the southwest at 5 m sec^{-1}. The wind backed through southerly at 1.5 km, reaching a speed of 10 m sec^{-1}, to easterly at 8 km, and westerly at 9 km with speeds about 2 to 3 m sec^{-1}. The 0625Z winds veered from southeasterly at 6.4 km to westerly about 9.5 km; the wind speed in this altitude region was 2 to 4 m sec^{-1}, too small to give much significance to the differences in the directional structure. Between 10 and 16 km the wind was westerly or northwesterly, with maximum speed about 22 m sec^{-1} at 15 km. Above 18 km the winds were easterly again. The PVM-7 soundings (Figure 7) showed humidity structure similar to that in the earlier soundings. The freezing level was lower over Kwajalein, about 4.5 km, but higher over Roi-Namur, about 5.1 km. Wind at the surface was southwesterly at less than 4 m sec^{-1}. The wind backed to southeasterly about 6.7 km, with maximum speed about 13 m sec^{-1} at 4.3 km. The Roi-Namur sounding showed a layer of weak easterly flow between 7 and 8 km, then a veering to westerly flow about 10 km. The Kwajalein sounding showed only the veering above 7 km, but the speeds were less than 3 m sec^{-1} through this layer. Above 10 km the wind structure was similar to that observed earlier.

Observations from both aircraft confirmed the general characteristics of the weather system. Considerable convective activity was present in the clouds prior to about 0000Z, as evidenced by sharp fluctuations in the water content profiles and by the presence of rimed crystals in the highest parts of the clouds. Some convection was detected later, particularly during the period 0600 to 0830Z, but the clouds were generally more stratiform at the times of the reentries.

3. AIRCRAFT WEATHER OBSERVATIONS

Weather reconnaissance operations and quantitative cloud sampling were conducted by the AFSWC C-130E and the Cessna Citation jet. The cloud physics instrumentation on the C-130E was under the direction of the Convective Cloud Physics Branch of the AFCRL Meteorology Laboratory. The instrumentation is described in Appendix A and illustrated in Figure 8. Similar instruments were installed on the Citation by MRI. The C-130E operated below 9 km, and the Citation up to 12 km. Their operations on 12 Oct 1974 are summarized in Tables 1 and 2.

The principal instruments on both aircraft were the PMS probes, which measured particle sizes to generate particle size spectra. The probes on the Citation covered the ranges from 1 to 31 μm (axially scattering spectrometer), 28 to 310 μm

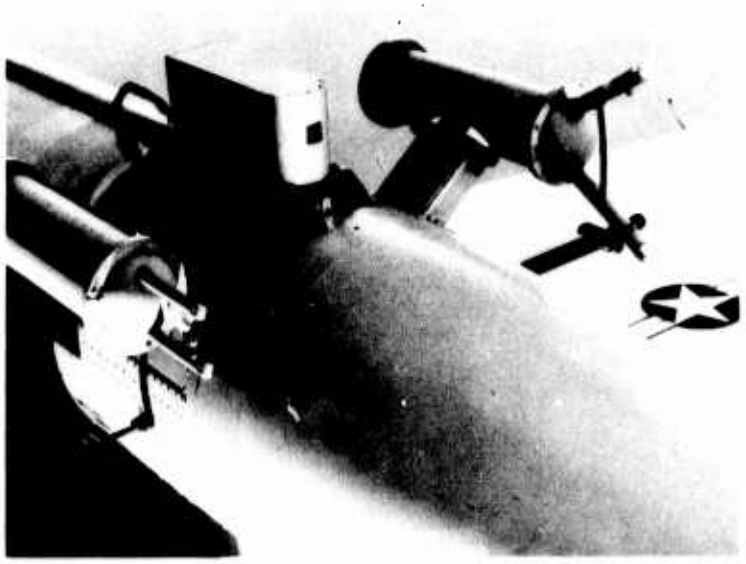

Figure 8. Instrumentation Pod Under Right Wing of C-130E (No. 40571). Instruments of pod (counterclockwise from upper left) are axially scattering spectrometer, precipitation particle spectrometer, foil sampler, cloud particle spectrometer, and Johnson-Williams liquid water content indicator.

Table 1. C-130E Operations at Kwajalein, 12 October 1974

Time (GMT)	Pressure (k ft)*	Altitude (km)	Remarks
0112-0153	17-25	5.2-7.6	Ascent in reentry corridor
0223-0239	25	7.6	Cloud sampling 200 km E of Kwajalein
0244-0302	23	7.0	
0305-0328	23-17	7.0-5.2	Cloud sampling 70-100 km ENE of Kwajalein
0334-0339	17	5.2	
0339-0440	17-29	5.2-8.8	Ascending, 30-40 km NE of Kwajalein
0632-0728	12.5-28	3.8-8.5	Ascending, 40-80 km ENE of Kwajalein
0831:45-0839:40	29-12	8.8-3.7	Descent in reentry corridor
0940:45-0944:30	12	3.9**	Correlation sampling with MPS-36 and ALCOR
0949:10-0952:20	15	4.9**	
0956:50-0959:55	18	5.8**	
1005:10-1008:05	21	6.8**	
1013:40-1016:30	24	7.8**	
1023:55-1026:35	27	8.8**	

*Altitudes in kft from aircraft flight records
**Altitudes from ALCOR tracking data

Table 2. Citation Operations at Kwajalein, 11 to 12 October 1974

Time (GMT)	Pressure altitude (k ft)	Computed altitude (km)	Remarks
2115-2315			Weather reconnaissance
2317-2331	38-15	12.5- 4.7	Cloud sampling in reentry corridor
2337-2354	15-30	4.7- 9.9	
0316-0343	15-30	4.5-10.1	Cloud sampling in reentry corridor
0412-0426	30-20	11.8- 6.6	
0435-0451	20-30	6.8-10.3	
0453-0505	30-12	10.3- 4.1	
0630-0700	15-30	4.6-10.4	Cloud sampling in reentry corridor
0717-0726	35-20	11.8- 6.5	
0730-0744	20-30	6.6- 8.9	
0827-0835	30-18	10.2- 5.8	

(optical array cloud particle spectrometer), and 234 to 3100 μm (optical array precipitation spectrometer). Each probe recorded particle counts in 15 channels, representing approximately equal size increments within the respective size ranges. The Citation carried a Formvar particle replicator (MRI Model 1203B) to provide a continuous record of the types of hydrometeors encountered by the aircraft. Its operation was similar to that of the replicator on the C-130E. The Citation also carried a MRI Model 1220 foil impactor. The particle shape data are used to convert the measured one-dimensional size spectra to spectra of equivalent melted diameters. From these spectra are derived the water content, proportional to the third moment of the spectrum, and the reflectivity factor, equal to the sixth moment of the spectrum.

Flight passes by the C-130E in conjunction with ALCOR weather measurements, using the link-offset mode, were designed to yield correlations of water content as derived from the aircraft and reflectivity factor measured by radar. These followed the flight paths shown in Figure 9. The reflectivity factors computed from the PMS data could be compared with values measured by radar as an independent check on the validity of the PMS data analysis. Correlations of Z and M derived from the aircraft data alone (in the absence of link-offset mode radar correlations) can also be used to interpret the radar weather data.

The cloud particle probe normally installed on the C-130E was replaced by a PMS precipitation probe that had been in the WB-57F used earlier in the Minuteman Natural Hazards Program. The purpose of the substitution was to obtain comparisons of spectral distributions and total water content as determined from the two probes. Studies of these data are underway at AFCRL and at MRI.

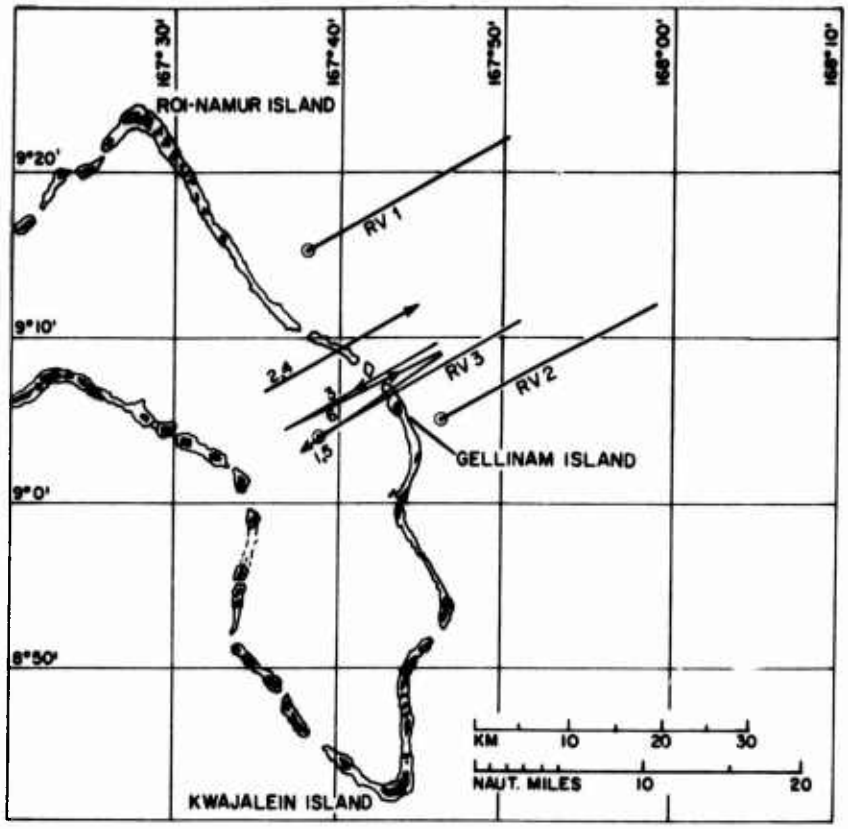

Figure 9. Reentry Trajectories and C-130E Flight Tracks for Correlation Operations. PVM-6 trajectories are indicated. Both of the PVM-7 trajectories were close to PVM-6 RV3. The aircraft flight tracks are numbered from the lowest altitude to the highest.

A holographic camera developed and operated by SAI[3] was installed on the Citation. This system utilized a pulsed ruby laser to produce three holograms per minute of a cylindrical sample volume 5 cm in diameter and 15 cm long. A three-dimensional image of the sample volume can be reconstructed from each hologram, and individual crystals can be observed with a resolution of about 50 μm. The holographic camera was operated throughout the July to October 1974 period, but due to failure of the electrical inverter was not operable on the PVM-6 and 7 mission day.

Observations during the first flight of the Citation indicated that there was considerable convective activity embedded in the thick cloud mass. The Citation did not reach the top of the clouds, which was above 12 km at this time. The general character of the ice water content profile was a gradual increase from about 0.05 gm m^{-3} at 10 or 11 km to about 0.3 gm m^{-3} at 5 or 6 km. More

variability was noted during the first flight than during the later ones, due to the convective activity prior to 0000Z. The crystal habit data accumulated by the replicator showed heavily rimed crystals at most levels during the first flight, consistent with the convective activity that carried liquid water droplets to high altitudes where they would have frozen onto the ice crystals. As the countdown progressed the weather system became more stratiform, and less riming of the crystals was observed. The crystal habits recorded by the replicator are shown in Figure 10, which spans the entire time of the Citation operations. The ice water content profiles remained fairly uniform during the second and third Citation flight, with maximum water content about 0.3 gm m^{-3} near 6 km. MRI reported that the cloud top height had decreased to near 11 km by the end of the third flight. This report is at variance with radar observations of clouds up to 12.5 km on the PVM-7 trajectories, and seems somewhat uncertain because the Citation performed relatively little sampling above 11 km. Examination of the C-130E camera films revealed the occurrence of a solar halo during the late afternoon, just prior to sunset. This observation indicated the presence of predominantly unrimed, uniform crystals above the flight level.

Values of ice water content and the radar reflectivity factor derived from the Citation PMS data were used to generate correlations of these quantities at different altitudes. The resulting equations are listed in Table 3 and illustrated in Figure 11. Data segments were selected from the profiles before and after each reentry, and were processed with some overlap in time to permit an evaluation of the transition from one crystal habit regime to the next. The Z-M equations used for the interpretation of the trajectory reflectivity data were selected on the basis of a comparison of the reflectivity factor computed from the PMS data with that measured by ALCOR in the same altitude-time interval (see Figure 16 in Section 4). These equations were then applied to the trajectory reflectivity data in corresponding altitude increments, with the equation for the highest altitude being applied up to the top of the cloud layer. The derived equation for the lowest altitude was applied down to the altitude of the $0^{\circ}C$ isotherm, and Eq. (8) was used in the lowest few kilometers. The results of this analysis are presented in Section 5.

Analogous correlation equations derived from the C-130E PMS data are listed in Table 4 and illustrated in Figure 12. These generally fall in the same area of the Z-M plot as those derived from the Citation data. The passes at the lowest altitudes (Passes 1, 3, and 4) yielded values of reflectivity factor much higher than those measured by ALCOR at these times. However, the equation from Pass 4 lies close to Eq. (8) on the diagram, justifying the use of Eq. (8) for computing water content below the freezing level.

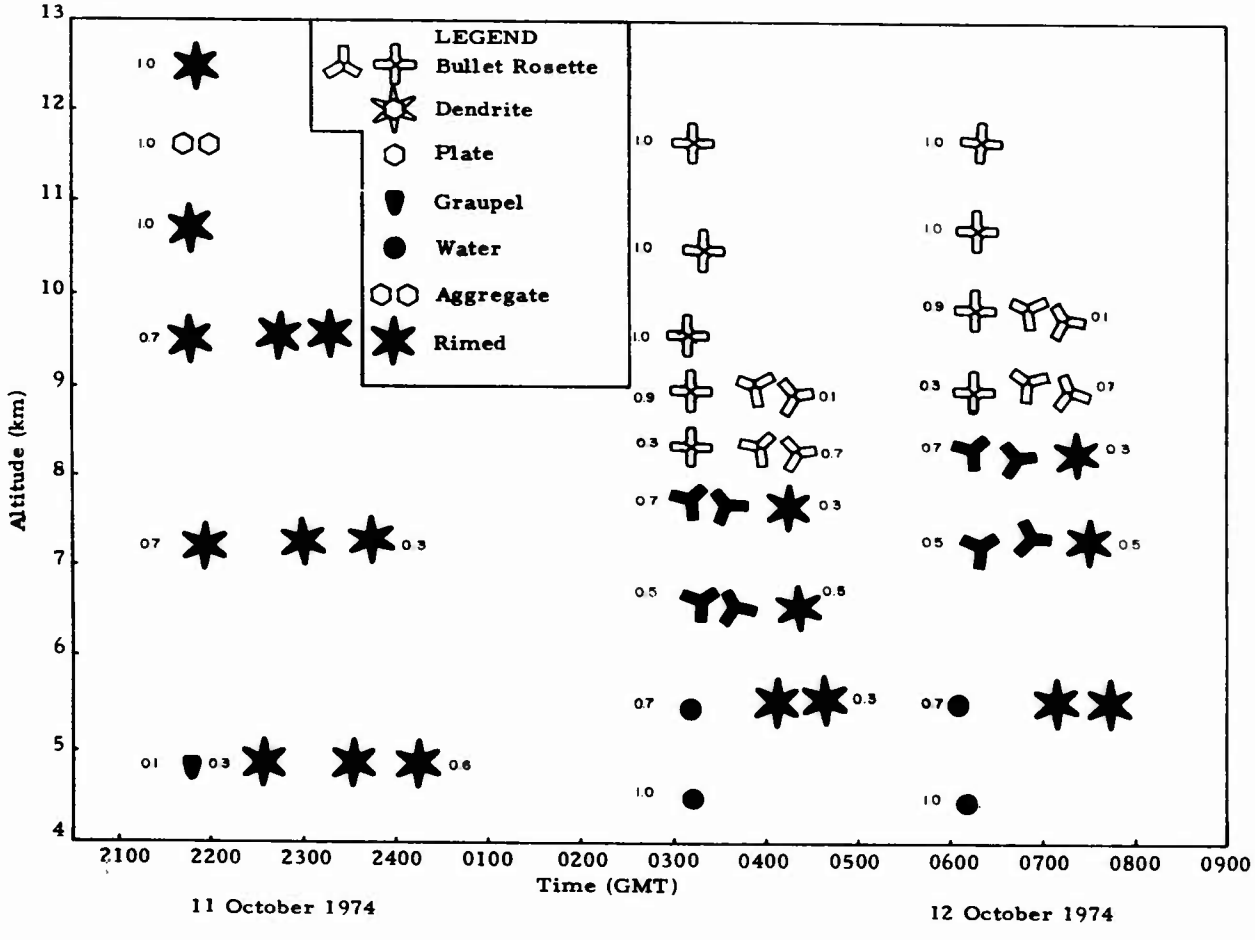

Figure 10. Time-Height Display of Crystal Habit Information Obtained From the MRI Formvar Replicator (courtesy of Jahnsen and Heymsfield[2]). Number beside each symbol indicates fraction of each particle habit at that altitude. Symbols in pairs represent aggregates of the particular crystal habit.

Table 3. Citation Cloud Data, 12 October 1974

Sequence Number	Time (GMT)	Altitude (km)	Mean Reflectivity (dBZ)	Crystal Habit*	$M\ (gm\ m^{-3}) = C\ Z\ (mm^6\ m^{-3})^E$	
					Coefficient (C)	Exponent (E)
1**	0456:34-0458:41	10.3- 9.6	2.0	BR	0.0151	0.410
2	0457:39-0459:45	10.3- 8.6	11.8	0.3 BR, 0.7 ABR	0.0221	0.400
3	0458:43-0502:57	9.5- 5.6	12.7	0.5 ABR, 0.5 ARD	0.0191	0.621
4	0501:55-0504:33	6.5- 4.1	38.5	0.3 ARD, 0.7 R	0.0011	0.850
5**	0629:28-0633:42	4.6- 5.6	33.6	0.3 ARD, 0.7 R	0.0065	0.643
6**	0632:40-0640:00	5.3- 7.3	14.8	0.5 ABR, 0.5 ARD	0.0359	0.424
	0640:02-0647:02	7.3- 8.6	13.4		0.0240	0.529
7**	0645:59-0654:00	8.4- 9.5	13.6	0.3 BR, 0.7 ABR	0.0340	0.318
8	0653:27-0700:00	9.5-10.3	16.3	BR	0.0112	0.553
9**	0716:55-0721:00	11.8- 9.8	11.6	BR	0.0076	0.569
10**	0720:39-0722:00	10.0- 9.2	12.5	0.3 BR, 0.7 ABR	0.0081	0.577
11**	0722:16-0727:02	9.0- 6.6	9.9	0.5 ABR, 0.5 ARD	0.0077	0.755
12	0828:23-0830:00	9.7- 8.7	15.9	BR	0.0105	0.443
13	0829:27-0831:00	9.0- 8.0	11.4	0.3 BR, 0.7 ABR	0.0111	0.474
14	0831:04-0835:00	7.9- 5.8	11.4	0.5 ABR, 0.5 ARD	0.0066	0.795

*Crystal habits: BR = Bullet rosettes, ABR = Aggregates of bullet rosettes, ARD = Aggregates of rimed dendrites, R = Rain

**Designates Z-M equation used in trajectory analysis

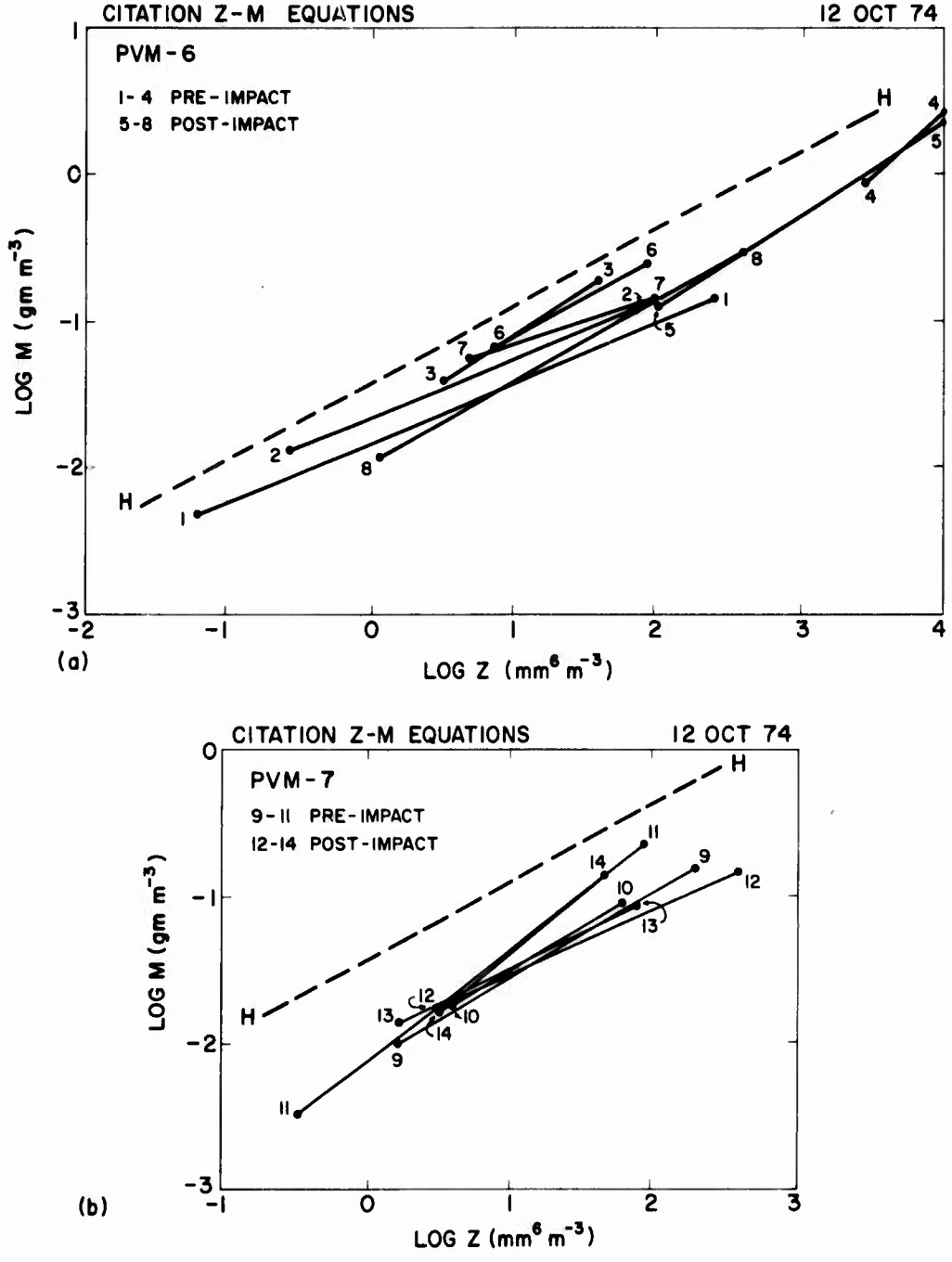

Figure 11. Correlations of Reflectivity Factor and Water Content Derived From Citation PMS Data. Numbering of correlation lines corresponds to that in Table 3. Correlations 1, 5, 6, and 7 were used to interpret the PVM-6 trajectory radar data. Correlations 9, 10, and 11 were used to interpret the PVM-7 trajectory radar data. Line designated "H" is Eq. (7), used for the preliminary interpretation of the ALCOR weather data.

Table 4. C-130E Cloud data, 12 October 1974

Sequence Number	Time (GMT)	Altitude (km)	Crystal Habit	$M\ (gm\ m^{-3}) = CZ\ (mm^6\ m^{-3})^E$	
				Coefficient (C)	Exponent (E)
1	0112:30-0116:45	5.2	Wet snow	0.0150	0.500
2	0123:00-0127:40	5.8	Large snow	0.0045	0.612
3	0328:10-0331:00	5.2	Rain	0.2681	0.140
4	0629:30-0632:00	4.3	Rain	0.0033	0.543
5	0641:00-0644:15	5.5	Wet snow	0.0025	0.709
6	0646:00-0648:30	6.1	Large snow	0.0124	0.637

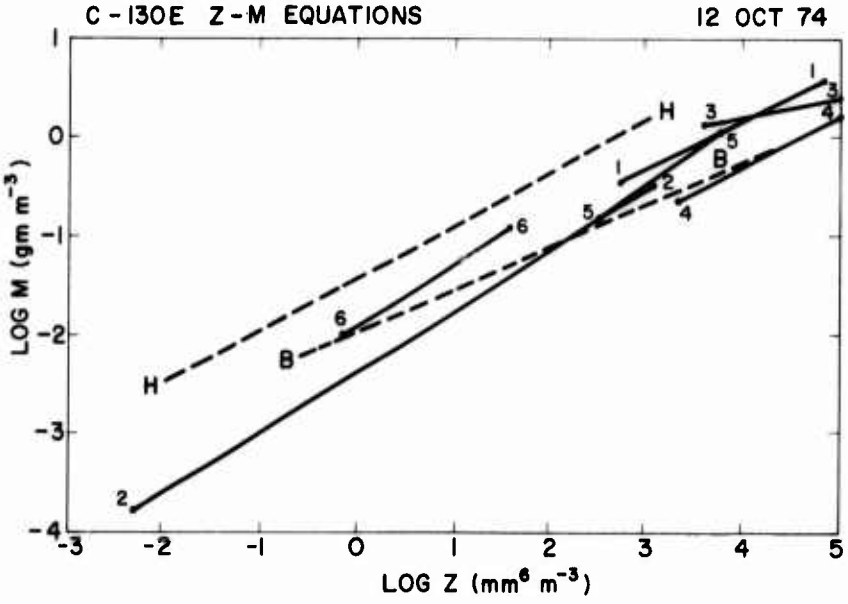

Figure 12. Correlations of Reflectivity Factor and Water Content Derived From C-130E PMS Data. Numbering of lines corresponds to that in Table 4. Line designated "B" is Eq. (8), used for the interpretation of ALCOR data below the freezing level.

4. ALCOR WEATHER OBSERVATIONS

Weather data were recorded by ALCOR throughout the July to October 1974 period while the Weather Team was at KMR. Operations in support of the PVM-6/PVM-7 weather documentation are summarized in Table 5. The weather data evaluation involved the PRESS B-6 tape radar cross-section data and the SPA-40 RHI display that were described in previous reports in the AFCRL/Minuteman series. The details of the B-6 data processing are presented in Appendix B. The radars principally involved in these operations were ALCOR and TRADEX, shown in Figure 13.

In addition to the data recorded on the B-6 tape, data were recorded at ALCOR in the same manner as for previous missions. The ALCOR data tapes were processed by Lincoln Laboratory and provided to AFCRL as calibrated radar signal values at 170 range gates spaced across a 2.5-km data window. These yielded a two-dimensional view of the weather structure along the trajectories. Final processing and analysis of these data were done by ERT programmers and AFCRL scientists. The flow of the radar weather data, and related data and communications, is shown in Figure 14.

The reflectivity factor Z ($mm^6\ m^{-3}$) was computed by the equation

$$Z = C\,\sigma/r^2 \tag{4}$$

or

$$dBZ = 10 \log C + 10 \log \sigma - 20 \log r \tag{5}$$

where σ is the cross-section (m^2), r is the range (km), and

$$C = \left[\frac{\lambda^4 \times 10^{10}}{\pi^5 \times |K|^2}\right]\left[\frac{8 \ln 2}{\pi\,\theta^2\, h \times 10^6}\right] , \tag{6}$$

where λ is the wavelength (5.29 cm), h is the nominal pulse length (37.5 m), θ is the beamwidth (5.24×10^{-3} rad), and $|K|^2 = 0.197$ for radar backscatter from ice crystals and 0.93 for backscatter from rain. Because ALCOR transmits a frequency-modulated "chirp" pulse, the nominal pulse length used in the above computation is not the transmitted pulse length; rather, it is a compressed pulse length corresponding to the output of a pulse-compression network in the radar receiver. Comparisons of chirp and constant-frequency radar weather data from

Table 5. ALCOR/PRESS Weather Support for PVM-6/7, 11 to 12 October 1974

RHI scans at 2309, 0324Z			
Trajectory weather scans	Area	Cld base (km)	Cld top (km)
2031-2035	A	< 1.5	14
2310-2320	A, B, D''	< 1.5	14
0148-0152	A	1	13
0341-0355	A, B, D''	1	13
PVM-6 Mission scans	RV	Cld base	Cld top
0517:27-0518:26	3	1.9	12.2
0522:56-0523:58	3	1.9	12.4
0524:18-0525:19	1	< 1.2	11.8
0525:36-0526:39	2	< 1.0	12.5
0526:50-0527:10	Vert		
0527:36-0528:39	3	1.9	12.4
0528:56-0529:59	1	< 1.2	11.8
0530:16-0531:18	2	< 1.0	12.5
0531:30-0531:47	Vert		
Trajectory weather scan	Area	Cld base	Cld top
0700-0701	A	< 3	11.5
PVM-7 Mission scans	RV	Cld base	Cld top
0759:11-0759:58	2	< 3.1	11.9
0804:25-0805:13	2	< 3.1	12.3
0805:37-0806:26	1	< 2.9	12.1
0806:36-0807:04	Vert		
0807:23-0808:09	2	< 3.2	12.1
0808:35-0809:22	1	< 3.0	12.4
0809:34-0810:00	Vert		
RHI scans at 0934, 1028Z			
Aircraft correlations		Alt (km)	Hdg (deg)
0939:15-0944:39		3.9	238
0948:51-0952:33		4.9	058
0956:23-0959:56		5.8	238
1004:34-1008:11		6.8	058
1013:27-1016:38		7.8	238
1023:34-1026:40		8.8	058

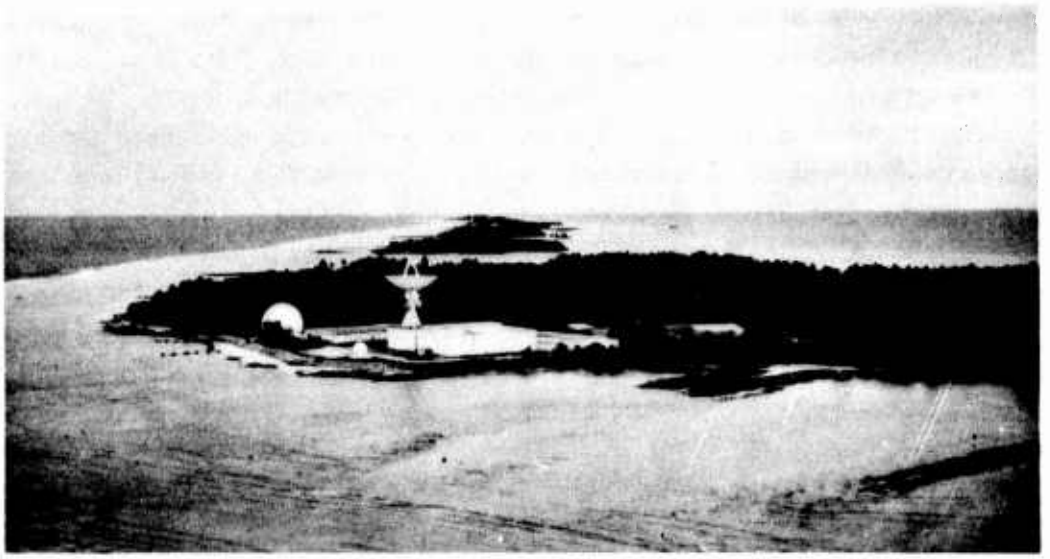

Figure 13. Lincoln Laboratory Radars at Kwajalein Missile Range. View is toward the southeast across the eastern part of Roi-Namur Island. ALCOR antenna is under dome at left, and TRADEX radar antenna is mounted on building in center. PRESS Control Center and computer are adjacent to TRADEX buildings.

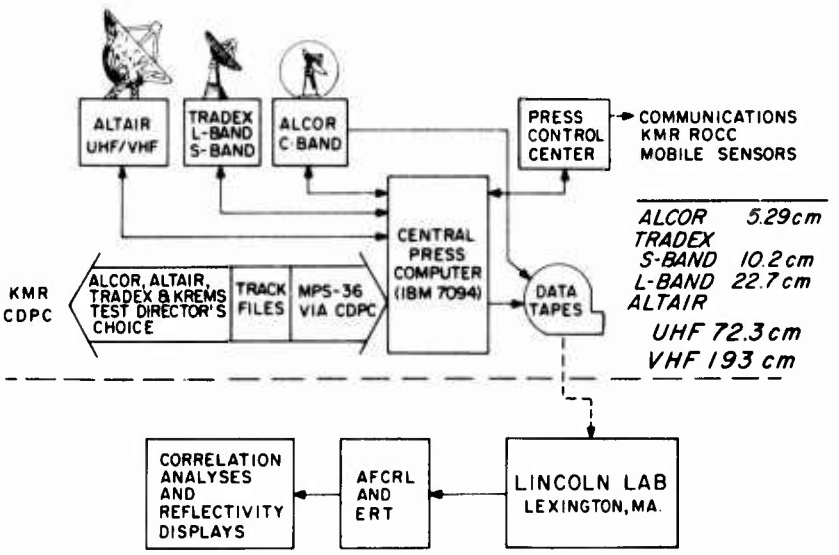

Figure 14. Radar Weather Data Flow Diagram. ALCOR is the principal weather sensor, with TRADEX S-band as backup. TRADEX L-band and ALTAIR were not used for weather measurements. ALCOR data are recorded on the PRESS B-6 tape for on-site processing of 1-sec averages, and also recorded directly for later processing at Lincoln Laboratory. Final processing and analysis are done by ERT programmers and AFCRL scientists.

the TTR-4 radar at Kwajalein[7] showed that the computational factor determined from Eq. (6) had to be increased by 3 dB for the chirp data. Thus 10 log C = 86.5 for the ALCOR observations above the freezing level and 79.8 in rain. We used only the received signals from the left circular polarization (opposite to the transmitted polarization) for this analysis, as these are 15 to 20 dB greater than those received on right circular polarization for weather echoes.

The quantity Z is the factor of the received signal power that is dependent only on meteorological parameters. For backscattered signals from particles much smaller than the radar wavelength, it is equal to the sixth moment of the particle size spectrum and, thus, is not a direct measure of the water content that is proportional to the third moment, or the volume. The relation of reflectivity to water content depends on the spectrum of ice crystals or water drops in a cloud. For preliminary estimates of water content, used for pre-mission forecasting and for the quick-look post-mission briefing, we used a Z-M equation appropriate to ice crystals[8] above the freezing level:

$$M = 0.038\ Z^{0.529} \quad . \tag{7}$$

Below the freezing level, we used a Z-M equation appropriate to tropical rain that was derived from equations presented by Battan[9]:

$$M = 0.011\ Z^{0.43} \quad . \tag{8}$$

(It should be noted that this Z-M equation was derived from surface observations, and is therefore not strictly applicable to observations in clouds; however, it is useful for preliminary estimates of the cloud water content.) One of the key objectives of the data analysis was the derivation of Z-M equations from the aircraft and radar data taken close to the time of the mission, to be used for interpreting the radar data recorded on the trajectories after the reentries.

Pre-mission weather reconnaissance was conducted with the aid of the RHI display and the B-6 data. Photographs of the RHI display, shown in Figure 15, were used to obtain cloud layer heights and cell locations. A scan at 2309Z toward the northwest (upwind at most levels) showed the cloud tops near 13 km,

---

7. Metcalf, J.I., Barnes, A.A., Jr., and Nelson, L.D. (1975) Water content and reflectivity measurement by "Chirp" radar. 16th Radar Meteor. Conf., Amer. Meteor. Soc., 492-495.

8. Heymsfield, A.J. (1973) The Cirrus Uncinus Generating Cell and the Evolution of Cirriform Clouds, Ph.D. Thesis, The University of Chicago.

9. Battan, L.J. (1973) Radar Observation of the Atmosphere. The University of Chicago Press.

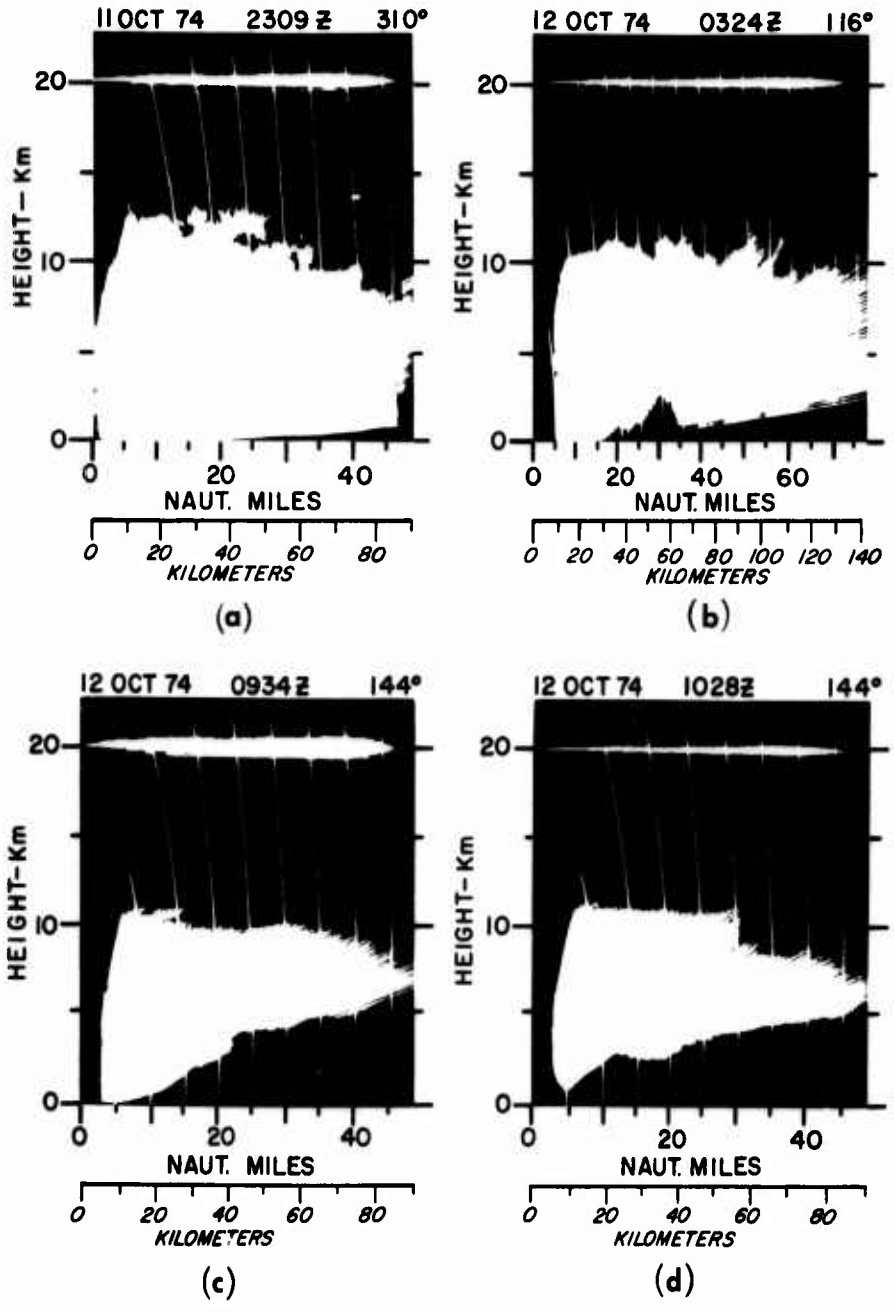

Figure 15. ALCOR RHI Scans During PVM-6 and PVM-7 Operations. Range markers are at 5 nmi (9.3 km) intervals. Height marker is at 20 km. (a) View toward the northwest at 2309Z shows thick cloud layer extending to about 13 km; signal intensity is too high to reveal convective structure. (b) View toward the reentry corridor at 0324Z shows cloud top near 12 km, with precipitation streamers evident in the highest few km. (c and d) During the post-mission aircraft sampling operations the cloud top is more uniform and slightly lower than earlier; sharp cloud base at 3 to 4 km altitude indicates the absence of precipitation as the cloud layer begins to dissipate.

with some evidence of convective activity. Closer to the time of PVM-6 reentry, the clouds in the reentry corridor extended only to 11 or 12 km, although the convective activity was still discernable. After PVM-7 the RHI showed that the clouds were more stratiform, with tops near 11 km.

Trajectory scans made prior to the missions were of limited usefulness for forecasting, due to an error in the PRESS program that was discovered later. These scans were taken at fairly regular intervals throughout the countdowns. With the recomputed Z values, it was possible to construct the time-height reflectivity display shown in Figure 16. The values of Z in the lower part of the figure are somewhat uncertain due to the difficulty of discriminating between ice and liquid water particles. However, the upper part of the figure compares favorably with reflectivity values computed from the Citation PMS data. The top of the radar-detectable cloud, initially about 15 km, dropped to about 13 km for most of the pre-mission period. The sharp drop in cloud top height prior to PVM-7 reentry and the decrease in reflectivity at all levels after 0730Z indicated the dissipation of the weather system that was occurring about this time.

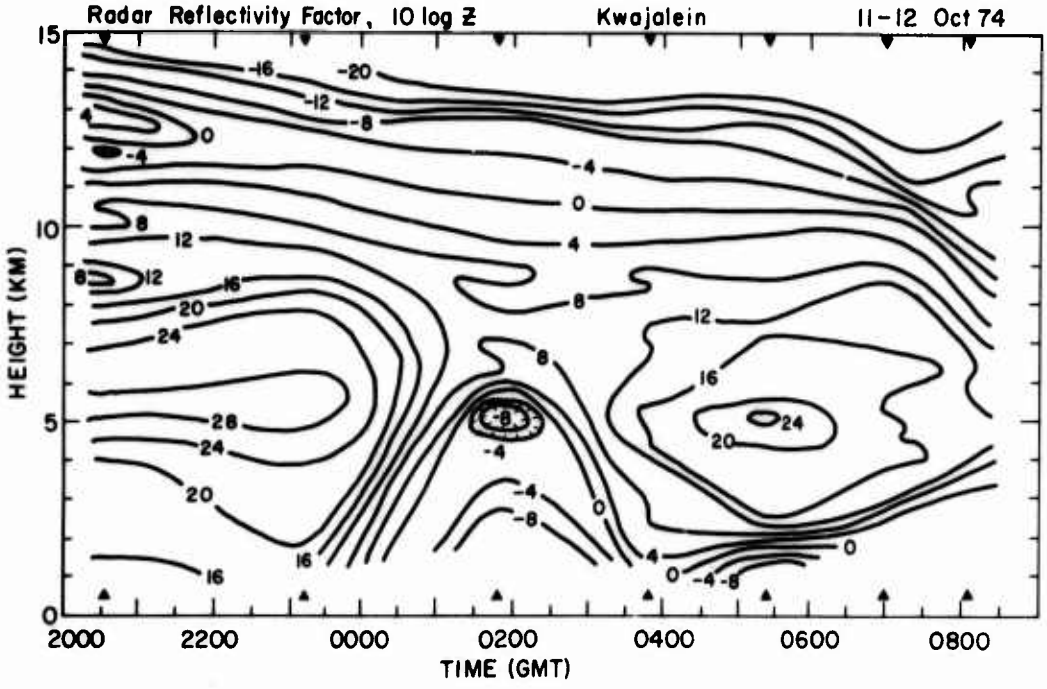

Figure 16. Time-Height Display of Radar Reflectivity Factor Z During PVM-6 and PVM-7 Operations. Contours are of 10 log Z (dBZ), with Z in $mm^6\ m^{-3}$. Low-altitude features such as the minimum at 0200Z may be due to small-scale variations in the cloud structure. Contours above 9 km altitude show gradual decrease in the cloud top height during the observational period. Onset of dissipation of the clouds is indicated by sharp decrease in height of contours after 0700Z.

Radar weather data along the PVM-6 trajectories are shown in Figures 17 through 22. A scan was made down the RV3 trajectory just prior to impact. Following the reentry a sequence of scans was made, once down each trajectory from about 20 km to near 1 km and once vertically over the radar from 6 to 20 km. This sequence was repeated to provide a time history of the weather on the trajectories. The vertical scans were intended to reveal high thin layers that might be too weak to appear in the trajectory scans, since the minimum detectable signal level increases as the square of the slant range.

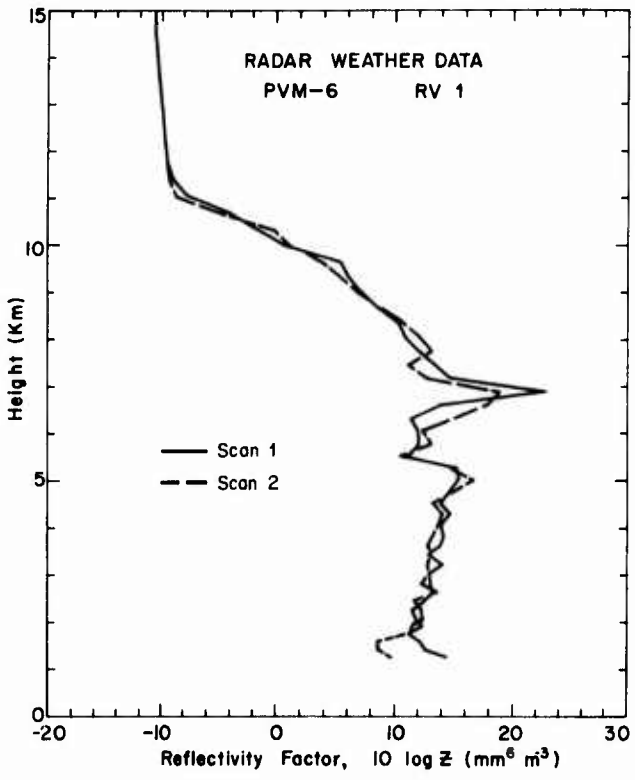

Figure 17. Profiles of Radar Reflectivity Factor Z on PVM-6 RV1 Trajectory. These are derived from the PRESS B-6 data and presented in logarithmic form (dBZ), with Z in $mm^6\ m^{-3}$. The two scans, 5 min apart, show the nearly steady weather structure following the reentry. Reflectivity values plotted above 12 km are the minimum signal levels for the PRESS B-6 data; for this mission these are abnormally high, due to a technical problem in the data link, and prevent a true determination of cloud top from this profile.

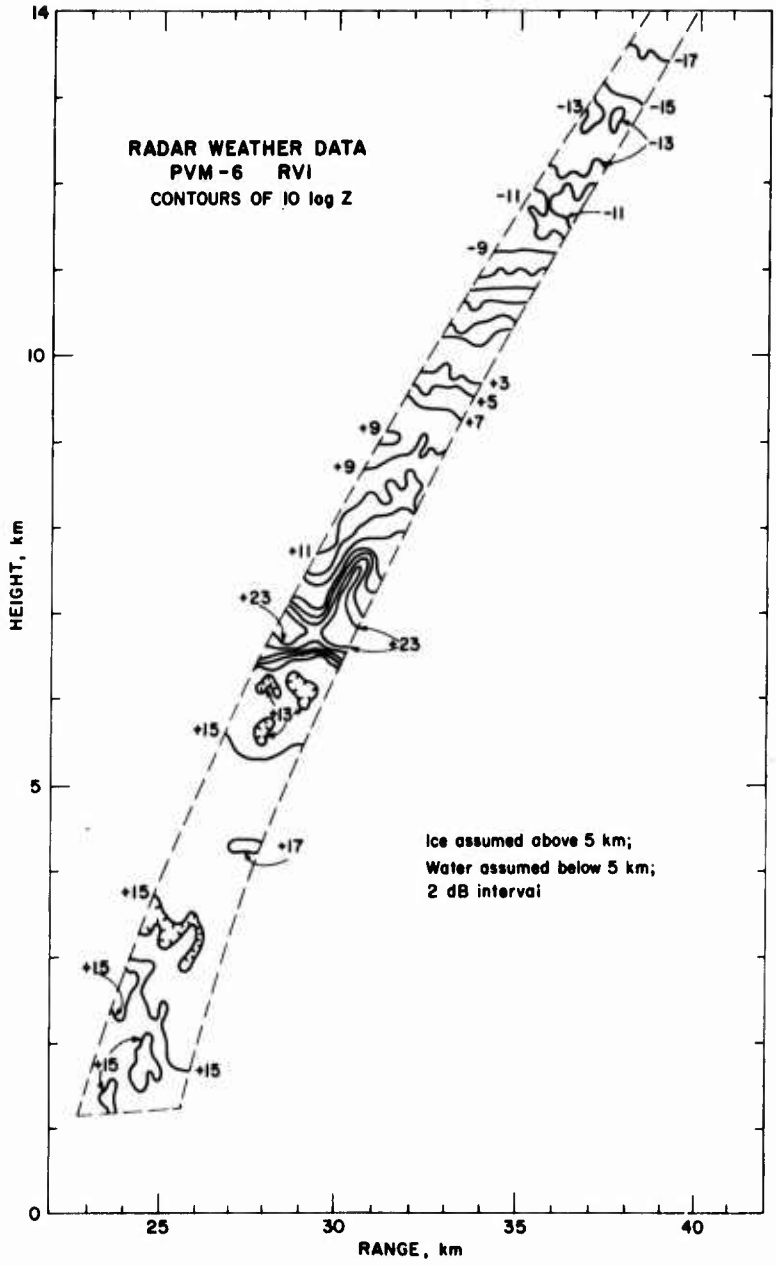

Figure 18. ALCOR Scan of PVM-6 RV1 Trajectory at 0525Z, 12 October 1974. Contours are of 10 log Z (dBZ), with Z in $mm^6\ m^{-3}$. These values were derived from the original ALCOR data recorded across a 2.5-km interval in slant range. Nominal trajectory location is approximately 1/3 of the width of the array from the near-range side. Cloud top is near 13.5 km, and closed contours near 13 km show a secondary layer at the top of the cloud mass. Maximum reflectivity near 7 km is due to a precipitation cell embedded in the cloud. Reflectivity below the melting level is relatively uniform.

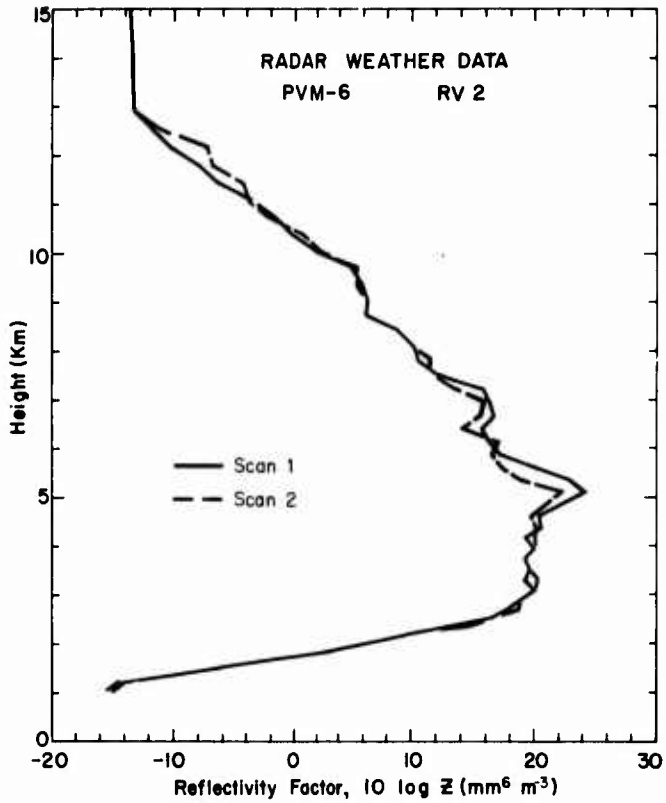

Figure 19. Profiles of Radar Reflectivity Factor Z on PVM-6 RV2 Trajectory. See text and legend of Figure 17 for details.

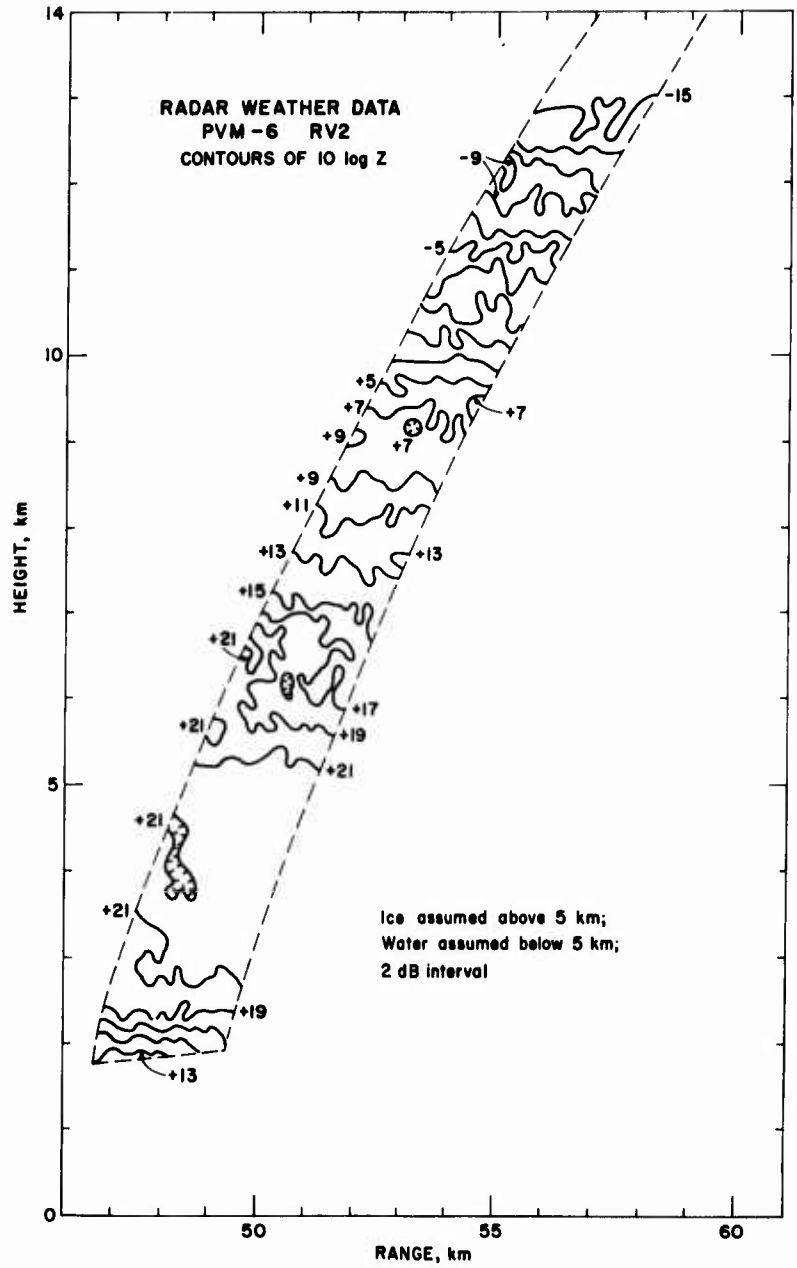

Figure 20. ALCOR Scan of PVM-6 RV2 Trajectory at 0526Z, 12 October 1974. Format is identical to that of Figure 18. Cloud structure shows considerable horizontal uniformity throughout the scan. Cloud top, somewhat above 13 km, was not detected on this trajectory, the furthest from ALCOR.

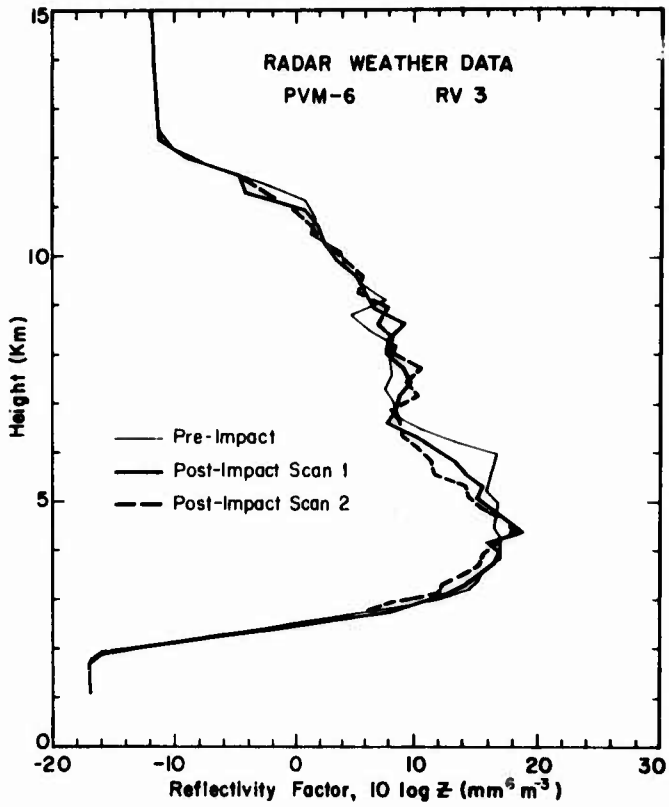

Figure 21. Profiles of Radar Reflectivity Factor Z on PVM-6 RV3 Trajectory. See text and legend of Figure 17 for details.

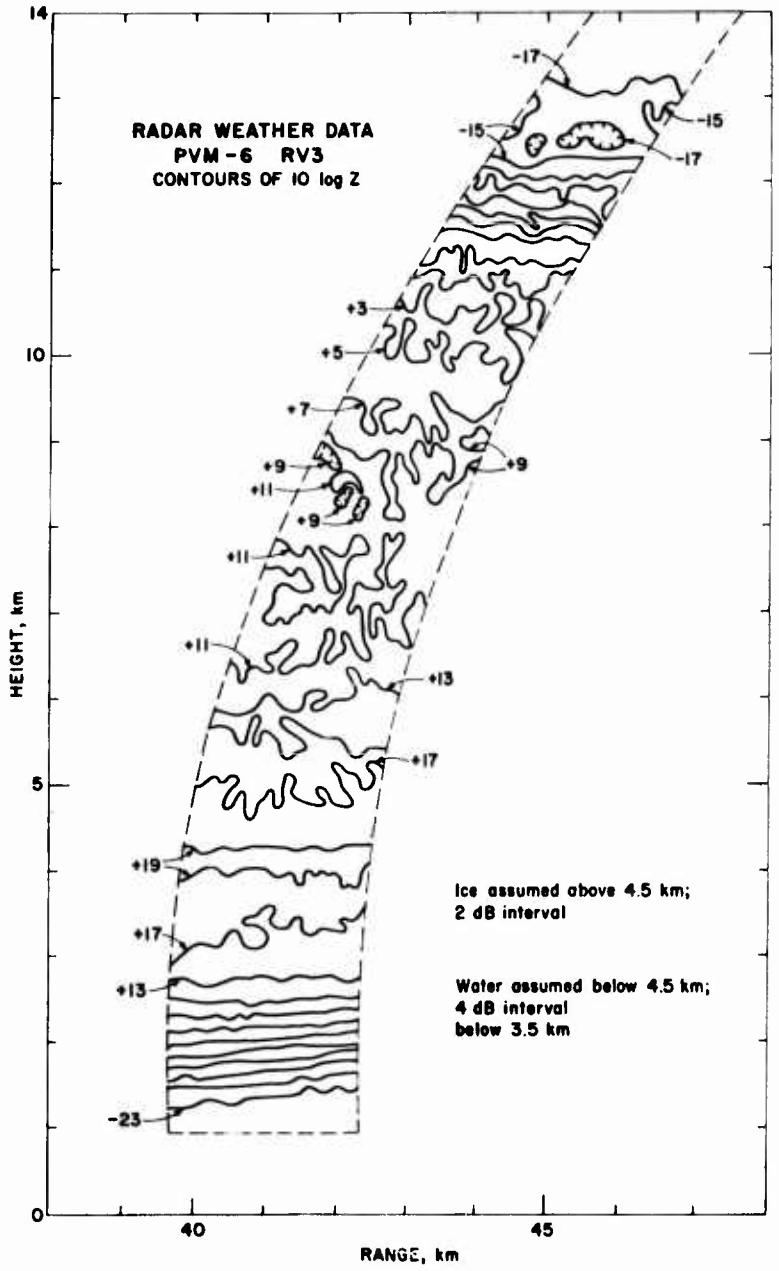

Figure 22. ALCOR Scan of PVM-6 RV3 Trajectory at 0523Z, 12 October 1974. Format is identical to that of Figure 18. Secondary cloud layer near 13 km is evident. Region between 9 and 6 km altitude shows considerable small-scale structure, but the variations of reflectivity are not large. Elsewhere the horizontal uniformity is remarkable.

The profiles in Figures 17, 19, and 21 were derived from the B-6 data, and show the remarkably small changes in the weather structure during the few minutes following the reentry. An ALCOR calibration problem resulted in the abnormally high minimum detectable signal levels at the tops of the scans, so that the true cloud tops were somewhat higher than implied by these figures. The general features are similar to those noted for the ice water content profiles obtained from the Citation. Cloud tops were near 12 or 13 km, and the reflectivity gradually increased to a maximum near 5 or 6 km. Cloud base was at or below 2 km. The two-dimensional representation of the weather structure near the trajectories is shown in Figures 18, 20, and 22, which were derived from the full ALCOR data tapes.

The RV1 scan (Figure 18) shows the cloud top near 13.5 km, with two reflectivity maxima at 13 and 12 km. Between 11 and 9 km the reflectivity increased, with relatively slight horizontal variations. Two strong maxima, probably due to a shaft of precipitation, were located just below 7 km. Below 6 km and into the rain region, the reflectivity was high, but quite uniform down to the bottom of the scan. The top of the clouds on the RV2 trajectory (Figure 20) was about 13 km. The weather structure was fairly uniform horizontally throughout the scan, with maximum reflectivity in the rain region below 5 km. The RV3 scan (Figure 22) shows the cloud top just above 13 km, with a weak layer at 13 km, above the principal cloud mass. The weather structure was quite uniform, especially near the cloud base, in the 1 to 3 km region. The maximum reflectivity was at 4 km, near the top of the rain region. The successive scans of the trajectories indicated minimal changes in the weather structure. The echo maximum at 7 km on the RV1 trajectory appeared smaller on the second scan, implying that it was moving away from the trajectory. It is probable that the reentry vehicle passed through this region of dense cloud or precipitation, but at a point where its vertical extent was relatively small.

The vertical scans (Figure 23) showed similar cloud structure to that observed on the trajectories, but with the top reaching to about 14 km. The reflectivity at this height indicates a water content of 0.0012 gm m^{-3}. Peak reflectivity values, corresponding to ice water content of 0.11 gm m^{-3}, were observed about 7 to 9 km.

Radar weather data along the PVM-7 trajectories are shown in Figures 24 through 27. The pre-impact scan was made on the RV2 trajectory, and the sequence of scans following the reentry was made as described above. The profiles in Figures 24 and 26 were derived from the B-6 data, and show only slight variation in the weather structure between the scans, which were 3 min apart. Maximum reflectivities were slightly lower than those observed on the PVM-6 trajectory scans. Figures 25 and 27, derived from the ALCOR data tapes, show the weather structure near the trajectories. The weather structure on the

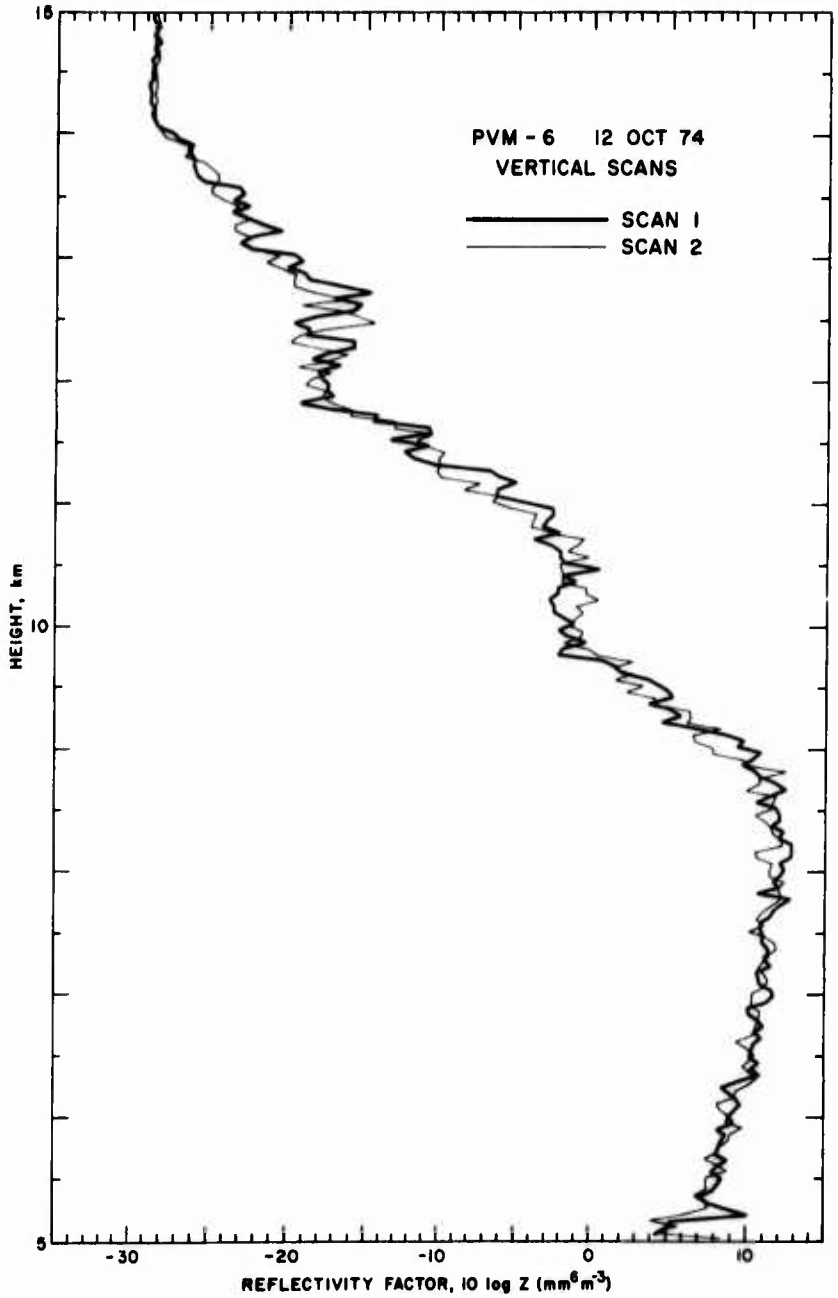

Figure 23. Profiles of Radar Reflectivity Factor Z on ALCOR Vertical Scans Following PVM-6 Reentry. Reflectivity values are comparable to those measured on the trajectories and illustrate the homogeneity of the cloud mass. These scans provide the best radar determination of the cloud top, near 14 km.

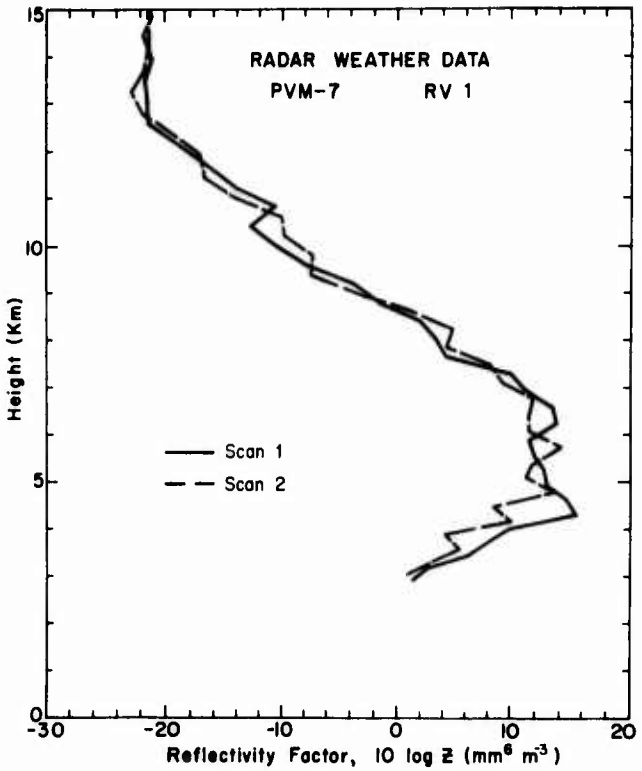

Figure 24. Profiles of Radar Reflectivity Factor Z on PVM-7 RV1 Trajectory. Format is identical to that of Figure 17. Reflectivity values above 13 km correspond to the ALCOR minimum detectable signal level. Reflectivity between 8 and 12 km is distinctly lower than at the time of PVM-6. Peak values between 4 and 7 km are comparable to those measured earlier.

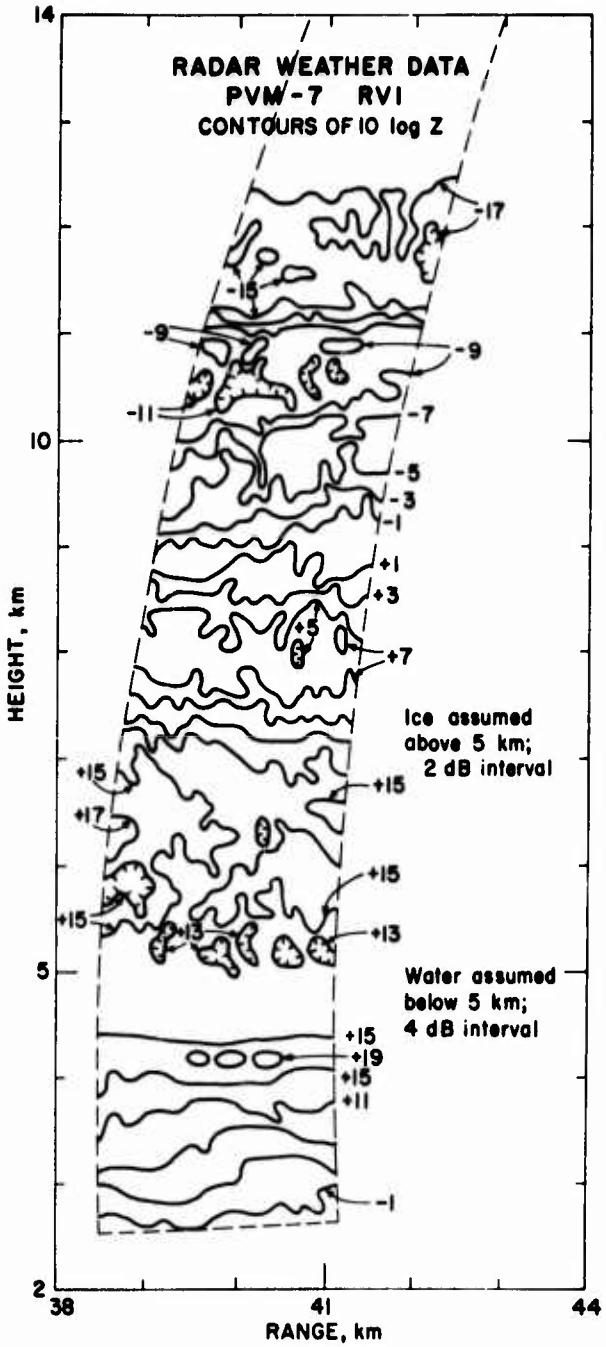

Figure 25. ALCOR Scan of PVM-7 RV1 Trajectory at 0806Z, 12 October 1974. Format is identical to that of Figure 18. Structure of cloud top is irregular, with local maxima near the trajectory at 11.5 to 12 km. Secondary layer is seen at 11 km, and reflectivity increases down the trajectory below 10.5 km.

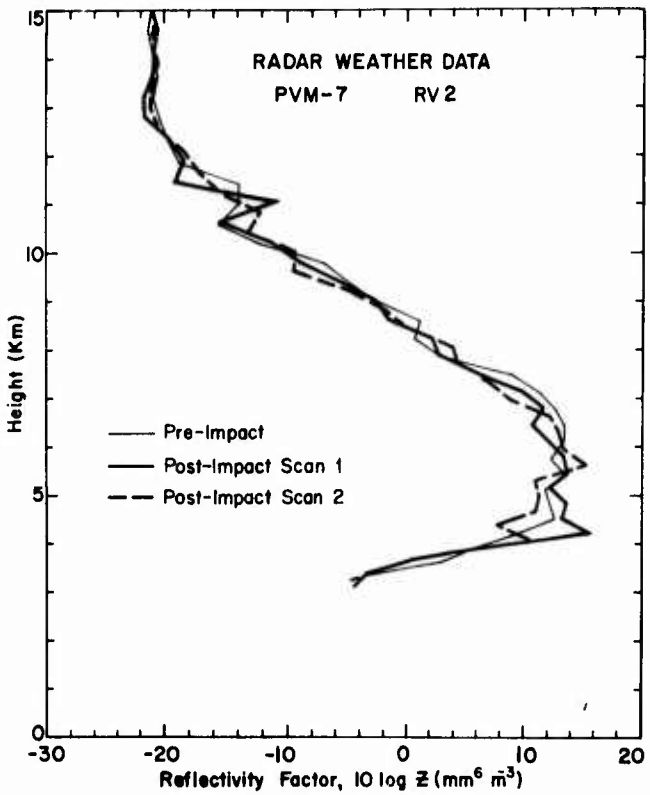

Figure 26. Profiles of Radar Reflectivity Factor Z on PVM-7 RV2 Trajectory. Format is identical to that of Figure 17, and features are similar to those in Figure 24.

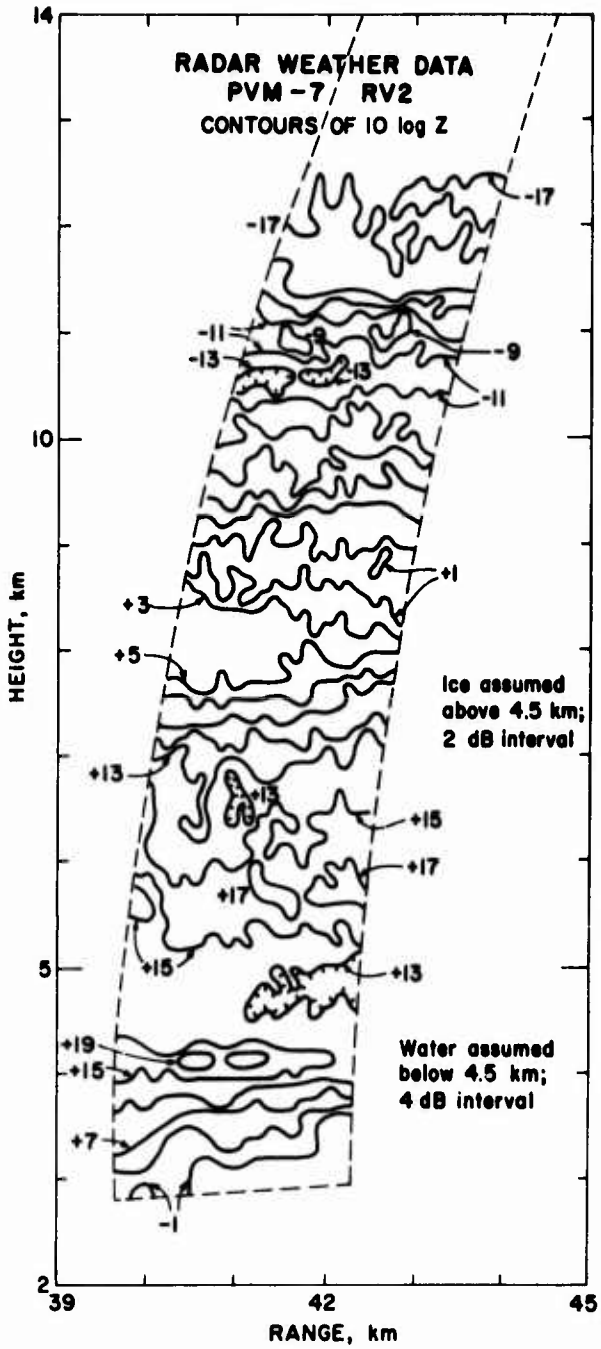

Figure 27. ALCOR Scan of PVM-7 RV2 Trajectory at 0805Z, 12 October 1974. Format is identical to that of Figure 18. Cloud structure is similar to that in Figure 25.

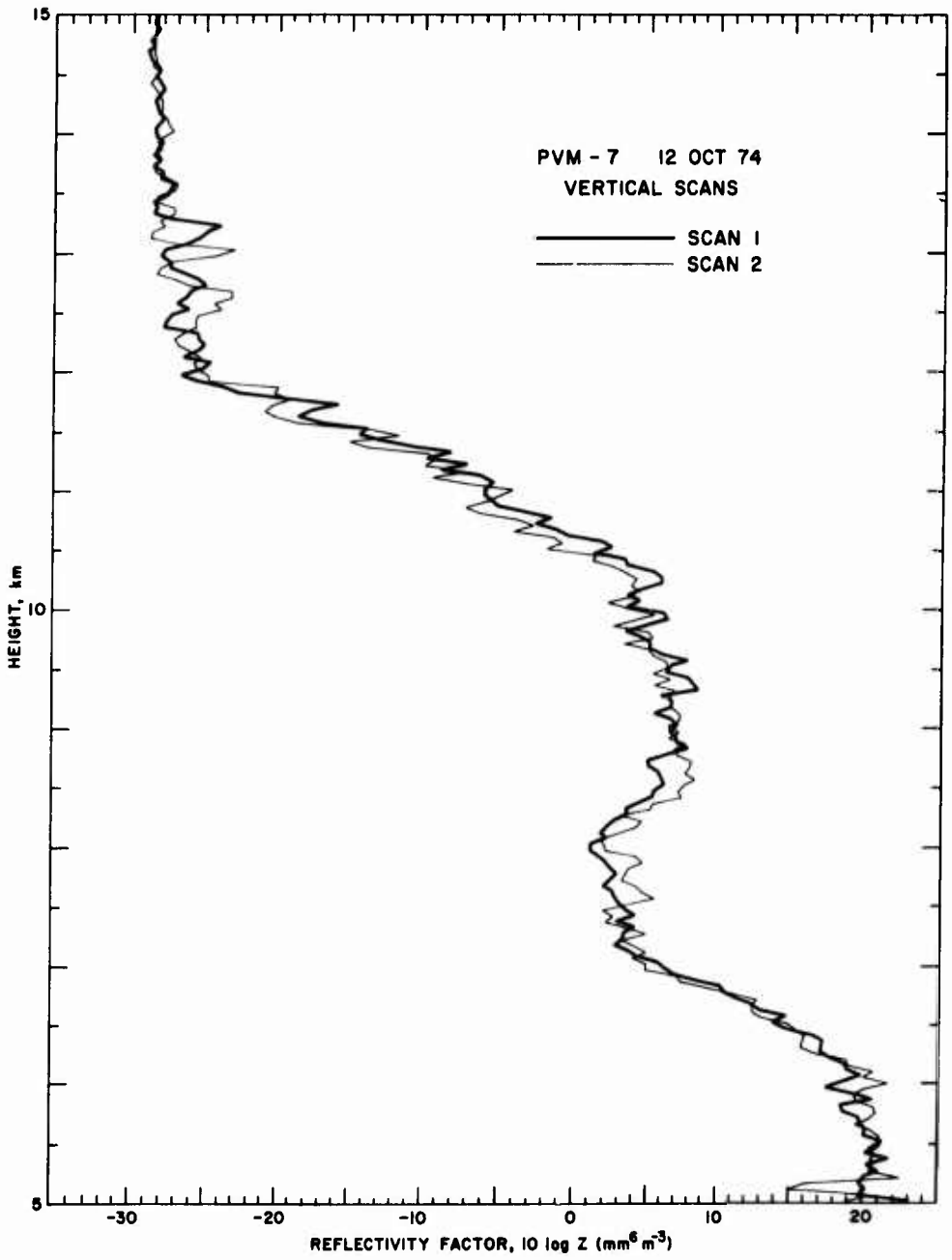

Figure 28. Profiles of Radar Reflectivity Factor Z on ALCOR Vertical Scans Following PVM-7 Reentry. Reflectivity maximum between 8 and 11 km differs from structure observed on the trajectories. Reflectivity values above 12 km are distinctly lower than those on the PVM-6 scans, and drop to the system noise level about 13.5 km.

two trajectories was quite similar. The cloud top was near 12.5 km, slightly lower than on the PVM-6 trajectories, and there was a distinct secondary layer near 11 km, which persisted throughout the scans. The second RV1 scan indicated that this secondary layer was merging with the primary cloud layer. The structure was quite uniform horizontally, with the reflectivity increasing to a maximum value just above 4 km. This maximum was probably the so-called "bright band," a phenomenon observed at the melting level as snow begins to melt and reflect more of the radar signal. Because of the complicated microphysics of the melting process, it is difficult to relate the "bright band" reflectivity to the water content. However, the water content profile can be interpolated across this layer.

The vertical scans (Figure 28) show the primary cloud layer extending to about 12 km, with some weak echoes up to about 13.5 km. Highest reflectivity, corresponding to ice water content of about 0.33 gm m^{-3}, was observed near 6 km.

Following the PVM-7 reentry, radar weather data were recorded in conjunction with the C-130E, in the link-offset mode. The purpose of these operations was to provide correlations of water content derived from the PMS data and reflectivity factor measured by radar. It has not been possible to complete this analysis, because of difficulties encountered in the PMS data reduction. For this reason the Z-M equations described in Section 3 were used to interpret the reflectivity data presented above.

5. SUMMARY AND CONCLUSIONS

The water content profiles encountered by the PVM-6 and PVM-7 reentry vehicles are shown in Figures 29 and 30, respectively. These were derived from the post-impact radar scans of the trajectories by means of the Z-M equations described in Section 3. The accuracy of these profiles is about ±4 dB, or a factor of 2.5. These limits are somewhat greater than those that would be applicable had we used correlation equations involving the ALCOR data. The profiles are generally in good quantitative agreement with those presented by MRI[2], although the radar is more capable of defining the precise geometry of the clouds along the trajectories.

The increments of the WSI above and below the freezing level are given in Table 6. The values of WSI we computed are less than those derived by MRI. In the case of PVM-6, their value (7.6) is well within the limits given above. For PVM-7 their value (7.2) seems to be excessively high. This is probably due in part to their technique of extrapolating the water content profiles and in part to the temporal and spatial variations in the weather structure. The ALCOR scans were

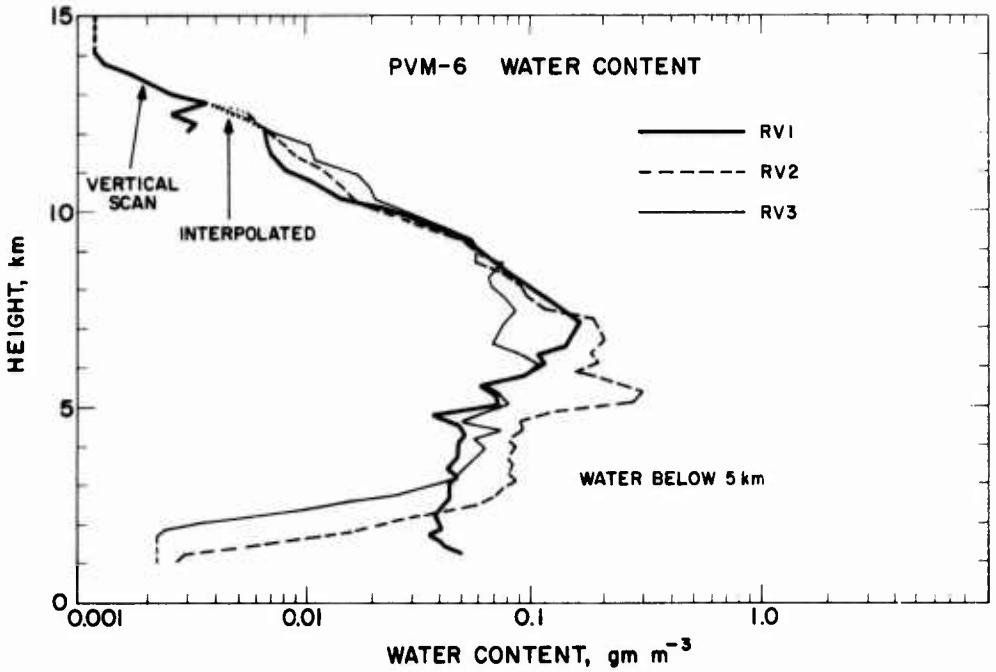

Figure 29. Profiles of Water Content on the PVM-6 Trajectories. These are derived from the reflectivity factor profiles (Figures 17, 19, and 21) by means of the Z-M equations shown in Figure 11. Reflectivity data from the vertical scans define the cloud top.

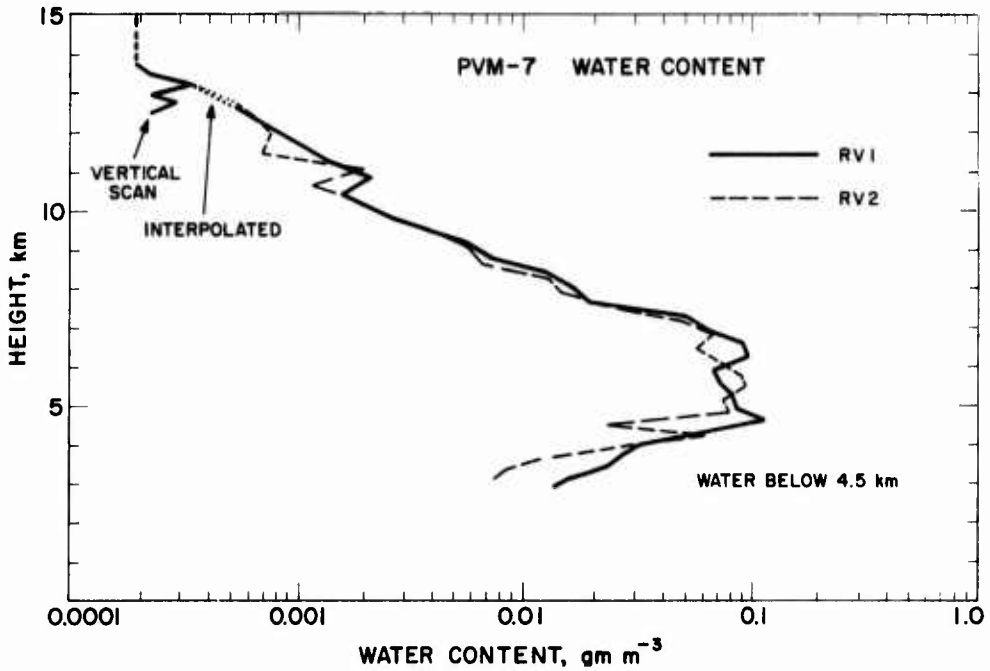

Figure 30. Profiles of Water Content on the PVM-7 Trajectories. These are derived from the reflectivity factor profiles (Figures 24 and 26) by means of the Z-M equations shown in Figure 11. Water content is less than on the PVM-6 trajectories, except in the 4 to 7 km layer.

Table 6. Weather Severity Index for PVM-6 and PVM-7

Trajectory	Above 5 km (ice)	Below 5 km (rain)	Total
PVM-6 RV1	3.8	0.5	4.3
RV2	5.0	0.9	5.9
RV3	3.1	0.5	3.6
PVM-7 RV1	1.7	0.3	2.0
RV2	1.4	0.2	1.6

taken just minutes after PVM-7 while the Citation descent was approximately 25 minutes after impact.

The weather system that produced these clouds developed along the ITCZ, and in somewhat more than a day produced a cloud mass that was remarkably uniform. During the early stages of its development there was considerable convective activity, typical of tropical weather systems, but the convection decreased as the system began to dissipate.

The critical factors in obtaining good quantitative weather documentation are the performance of the instruments and the difficulty of obtaining the data close to the time and place of the reentry. In the present case the aircraft-radar correlation operations did not yield usable results, due to technical reasons; however, had the analytical results been technically satisfactory, their applicability to the reentry trajectories, particularly of PVM-6 which was 4 to 5 hr earlier, would have been questionable because of the changes in the cloud characteristics during this time. The radar scans of the trajectories close to the time of impact were the key element in reconstructing the trajectory profiles of water content. Radar scans made throughout the countdown period enabled us to validate the results of the aircraft data analysis with respect to both the reentry profiles and the longer-term development of the weather system.

References

1. Wilmot, R.A., Cisneros, C.E., and Guiberson, F.L. (1974) High cloud measurements applicable to ballistic missile systems testing, 6th Conf. Aerosp. and Aeronaut. Meteor., Amer. Meteor. Soc., 194-199.
2. Jahnsen, L.J., and Heymsfield, A.J. (1975) High Altitude Ice Cloud Characterization: PVM-6, -7, and -8 Missions, MRI 75 FR-1350, Meteorology Research, Inc., Altadena, California.
3. Trolinger, J.D., Farmer, W.M., and Clayton, F.P. (1974) Development and Application of an Airborne Holography System and Particle Sizing Interferometer, SAI-74-511-TT, Science Applications, Inc., La Jolla, California.
4. Jahnsen, L.J. (1975) Utilization of SAMSO Airborne Holocamera for Cloud Physics Measurements, MRI 75 FR-1331, Meteorology Research, Inc., Altadena, California.
5. Gruber, A. (1972) Fluctuations in the position of the ITCZ in the Atlantic and Pacific Oceans, J. Atmos. Sci. 29:193-197.
6. USAF Environmental Technical Applications Center (1973) Monthly Cloud Climatology for Kwajalein, Marshall Islands. Project 7076, Report 7076A.
7. Metcalf, J.I., Barnes, A.A., Jr., and Nelson, L.D. (1975) Water content and reflectivity measurement by "Chirp" radar. 16th Radar Meteor. Conf., Amer. Meteor. Soc., 492-495.
8. Heymsfield, A.J. (1973) The Cirrus Uncinus Generating Cell and the Evolution of Cirriform Clouds, Ph.D. Thesis, The University of Chicago.
9. Battan, L.J. (1973) Radar Observation of the Atmosphere. The University of Chicago Press.
10. Church, J.F., Pocs, K.K., and Spatola, A.A. (1975) The Continuous Aluminum Foil Hydrometeor Sampler; Design, Operation, Data Analysis Procedures, and Operating Instructions, AFCRL-TR-75-0370, IP No. 235.

Appendix A

C-130E Instrumentation

Three one-dimensional particle spectrometers measure the sizes of hydrometeors encountered by the aircraft. These were built by Particle Measuring Systems, Inc., Boulder, Colorado. An axially scattering spectrometer measures particles in the range of 1 to 31 μm, and two optical array spectrometers cover the ranges 30 to 310 μm (cloud particle spectrometer) and 315 to 4287 μm (precipitation spectrometer). Each probe records particle counts in 15 channels representing approximately equal size increments within the range of sizes given above. By considering the probe geometry and the aircraft speed, these counts are converted into number concentrations that transform readily into a particle size distribution. An onboard display permits the operator to determine size distributions while in flight. Data from this instrument are also recorded on a digital, computer-compatible magnetic tape for post-mission analysis.

The foil sampler,[10] built by Meteorology Research, Inc., is a direct mechanical replicator consisting of a thin sheet of aluminum foil that is pulled, at constant speed, across a shuttered opening. Hydrometeors hit the foil and create imprints that are replicas of their size and shape. The foil replicator covers the range of sizes from 50 μm to 5 mm. Particles smaller than 50 μm will not make an imprint

---

10. Church, J.F., Pocs, K.K., and Spatola, A.A. (1975) The Continuous Aluminum Foil Hydrometeor Sampler; Design, Operation, Data Analysis Procedures, and Operating Instructions, AFCRL-TR-75-0370, IP No. 235.

on the foil. Analysis of the foil is a laborious process requiring the eyes and mind of an experienced analyst.

The Formvar replicator physically captures hydrometeors on a moving film that is coated with a fast-drying mixture of Formvar and chloroform. The drying rate is sufficiently fast that ice particles do not melt out of shape before the Formvar dries around them. Particles larger than 2 μm can be sampled. Replication of ice crystals is good up to about 500 μm; liquid droplets are replicated well only to about 50 μm diameter due to breakup of larger drops. Dry nitrogen is used to dry the coating and to provide positive pressurization of the instrument. This reduces fragmentation by reducing the particle speed at impact. The films are analyzed after each flight by means of a photo-analyzer (stop-motion) projector. This instrument was built by the Desert Research Institute of the University of Nevada.

The liquid water content indicator was built by Johnson-Williams Products, Mountain View, California. Water droplets strike one of two calibrated resistance wires of a balanced bridge. As the droplets absorb heat from the wire the bridge becomes unbalanced. The magnitude of the imbalance voltage is a measure of the LWC encountered. This instrument is designed to work in liquid clouds composed of droplets from 10 to 50 μm diameter, since larger droplets and solid particles have an unknown cooling efficiency. Therefore, this device is not useful in clouds containing rain, but it does detect super-cooled droplets in ice clouds and thereby provides information on riming.

The dewpoint / frostpoint temperature sensor is a thermistor mounted on a thermoelectrically cooled mirror that is maintained at the highest temperature at which dew or frost will form. As the reflectivity of the mirror is reduced by the film of dew or frost, a monitoring photoelectric circuit senses the change and regulates the cooling unit. The output of this instrument is a voltage proportional to the dewpoint (or frostpoint) temperature. This instrument was built by the Environmental Equipment Division of EG&G, Inc., Waltham, Massachusetts.

The Rosemont temperature probe is a high precision, rapid-response instrument. Its output is a voltage that varies as a function of dynamic heating (true airspeed) and density (altitude) as well as the actual temperature. The temperature probe was built by Rosemont, Inc., Minneapolis, Minnesota.

A pressure altimeter is used to determine the aircraft's operating altitude. Its output is a voltage proportional to the pressure altitude.

The Snow Stick is an aluminum rod that is used to determine ice crystal habit and size while flying through cirrus cloud or snow. At one end are four flat faces, painted black and marked with 1-cm squares. The rod is inserted through the side of the aircraft so that the sampling areas are 30 cm into the airstream. The operator can rotate the stick as necessary to bring each face perpendicular to the

airstream. As snow crystals impinge on the stick the flight director can make judgments as to the crystal size and type. The minimum detectable size is approximately 200 μm, unless the snow stick is brought inside the aircraft and viewed with an eyepiece to observe particles as small as 10 μm.

The time code generator provides a digital readout of Greenwich Mean Time (GMT) in hours, minutes, and seconds. This information is recorded on the data tape recorders and also displayed at each project-crew position within the aircraft.

The 16-mm nose camera is a time lapse camera controlled by the flight director. It is used to photograph cloud conditions for later analysis.

A voice tape recorder is used by all participants in the mission. Most recorded information comes from the flight director, but any crewman may record information and special observations.

The PDP 8/I computer processes digital data (PMS counts, time) or analog data (airspeed, heading, J-W LWC, altitude, temperature) in real time aboard the aircraft. The PDP 8/I was built by the Digital Equipment Corp., Maynard, Massachusetts.

Appendix B

Derivation and Processing of Press B-6 Data

From each radar pulse the four signal values in gates 51, 52, 53, and 54 (centered about the radar tracking point) were examined to determine the maximum. The maximum value from each pulse was stored, and an average of these was computed for each 1/10 sec (about 20 pulses). This average was transmitted to the PRESS computer in the form of encoded values of radar cross-section and recorded on the "B-6" tape. In cooperation with personnel at PRESS, we developed a program to average these values over 1-sec intervals and compute the reflectivity factor Z by Eq. (5). These 1-sec averages provided the data for the reflectivity profiles shown in Figures 17, 19, 21, 24, and 26 of the report. The program also computed ice water content M by Eq. (7) and WSI by Eq. (3) for purposes of pre-mission weather evaluation.

As will be described in a future report in this series, the reflectivity values computed from the B-6 data were approximately 0.8 dB low. This correction was not included in the reflectivity profiles shown above, and is not needed if the reflectivity data are interpreted by Z-M equations obtained from correlation of aircraft and ALCOR data. However, if Z-M equations derived exclusively from aircraft data or obtained from the scientific literature are used for the interpretation, then the correction is needed. The radar data were corrected as necessary for the derivation of the water content profiles shown in Figures 29 and 30.

List of Acronyms and Symbols

AFCRL	Air Force Cambridge Research Laboratories
AFSWC	Air Force Special Weapons Center
ALCOR	ARPA-Lincoln C-band Observables Radar
ALTAIR	ARPA Longe-range Tracking and Instrumentation Radar
ARPA	Advanced Research Projects Agency
CDPC	Central Data Processing Computer
DMSP	Defense Meteorological Satellite Program
EG&G	Edgerton, Germeshausen, and Grier, Inc.
ERT	Environmental Research and Technology, Inc.
FAA	Federal Aviation Administration
GMT	Greenwich Mean Time
ITCZ	Inter-Tropical Convergence Zone
KMR	Kwajalein Missile Range
KREMS	Kiernan Reentry Measurements Site
M	Water content (liquid or ice), gm m^{-3}
MRI	Meteorology Research, Inc.
NWS	National Weather Service
PMS	Particle Measuring Systems, Inc.
PPI	Plan Position Indicator
PRESS	Pacific Range Electromagnetic Signature Studies
PVM	Production Verification Missile
RHI	Range Height Indicator
ROCC	Range Operations Control Center

RV	Reentry Vehicle
SAI	Science Applications, Inc.
SAMSO	Space and Missile Systems Organization
SAMTEC	Space and Missile Test Center
TRADEX	Target Resolution and Discrimination Experiment
TTR	Target Tracking Radar
WSI	Weather Severity Index
Z	Radar reflectivity factor, $mm^6\ m^{-3}$
Z	Greenwich Mean Time